

Mapping 24 woody plant species phenology and ground forests phenology over China from 1951-2020

Mengyao Zhu¹, Junhu Dai^{1,2,3}, Huanjiong Wang¹, Juha M. Alatalo⁴, Wei Liu^{1,2}, Yulong Hao^{1,2}, Quansheng Ge^{1,2}

¹Key Laboratory of Land Surface Pattern and Simulation, Institute of Geographic Sciences and Natural Resources Research, Chinese Academy of Sciences, Beijing, 100101, China

²College of Resources and Environment, University of Chinese Academy of Sciences, Beijing, 101408, China

³China-Pakistan Joint Research Center on Earth Sciences, CAS-HEC, Islamabad, 45320, Pakistan

⁴Environmental Science Centre, Qatar University, Doha, 2713, Qatar

Correspondence to: Junhu Dai (daijh@igsnr.ac.cn); Quansheng Ge (geqs@igsnr.ac.cn)

Abstract. Plant phenology refers to the cyclic plant growth events, and is one of the most important indicators of climate change. Integration of plant phenology information is crucial for understanding ecosystem response to global change and modeling the material and energy balance of terrestrial ecosystems. Utilizing 24,552 in-situ phenological observations of 24 representative woody plants species from the Chinese Phenology Observation Network (CPON), we have developed maps delineating species phenology (SP) and ground phenology (GP) of forests over China from 1951-2020. These maps offer a detailed spatial resolution of 0.1° and a temporal resolution of 1 day. Our method involves a model-based approach to upscale in-situ phenological observations to SP maps, followed by the application of weighted average and quantile methods to derive GP maps from the SP data. The resulting SP maps for the 24 woody plants exhibit a high degree of concordance with in-situ observations, manifesting an average deviation of 6.9 days for spring and 10.8 days for autumn phenological events. Moreover, the GP maps demonstrate robust alignment with extant Land Surface Phenology (LSP) products sourced from remote sensing data, particularly within deciduous forests, where the average discrepancy is 8.8 days in spring and 15.1 days in autumn. This dataset provides an independent and reliable phenology data source for China on a long-time scale of 70 years, and contributes to more comprehensive research on plant phenology and climate change at both regional and national scales. The dataset can be accessed at <https://doi.org/10.57760/sciencedb.07995> (Zhu et al., 2023).

1 Introduction

Plant phenology, the discipline that examines the timing of plant life cycle events, emerges in response to the seasonal changes in climate and environmental conditions (Lieth, 1974; Schwartz, 2003). These events are pivotal stages in a plant's life, such as budburst, leaf unfolding, flowering, leaf coloring, and defoliation. Recognized as a sensitive biological indicator of climate change (Fu et al., 2015; Richardson et al., 2013), plant phenology is instrumental in understanding ecosystem responses to global change (Menzel et al., 2020), and is a significant factor in modeling the exchanges of matter and energy within terrestrial ecosystems (Keenan et al., 2014). The demand for extensive, long-term, and reliable plant phenology data

删除[伊洛。]: of great significance

删除[伊洛。]: the

删除[伊洛。]: of ecosystems

删除[伊洛。]: simulating

删除[伊洛。]: y

删除[伊洛。]: records

删除[伊洛。]: typical

删除[伊洛。]: map the

删除[伊洛。]: ,

删除[伊洛。]: with a spatial resolution of 0.1° and a temp [...]

删除[伊洛。]: A

删除[伊洛。]: upscaling

删除[伊洛。]: method was used

删除[伊洛。]: generate

删除[伊洛。]: SP maps from

删除[伊洛。]: y

删除[伊洛。]: were used

删除[伊洛。]: generate

删除[伊洛。]: maps

删除[伊洛。]: he validation shows that t

删除[伊洛。]: of

删除[伊洛。]: the

删除[伊洛。]: in

删除[伊洛。]: in

删除[伊洛。]: T

删除[伊洛。]: of forests have good agreement

删除[伊洛。]: by

删除[伊洛。]: 1: with an

is pronounced among researchers for effective biological monitoring and predictive studies. Although such data are now available from various sources (Piao et al., 2019; Tang et al., 2016), including in-situ observations (Templ et al., 2018), satellite remote sensing (Bolton et al., 2020; Dixon et al., 2021), and tower-based digital cameras (Richardson et al., 2018), harmonizing this information across broad spatial and temporal scales remains a significant scientific challenge, complicated by inconsistencies among data sources (Fisher et al., 2006; Park et al., 2021).

The practice of conducting manual, in-situ observations for species phenology (SP) boasts a rich history extending over several centuries (Aono and Kazui, 2008), yielding highly accurate data for specific plant species (Polgar and Primack, 2011). In 1963, the Chinese Academy of Sciences established the Chinese Phenology Observation Network (CPON), which stands as a benchmark for phenological data collection through its standardized, nationwide network, engaging numerous professional observers and an extensive repository of ground-based observations. CPON's repository, to date, encompasses over 1.2 million records for upwards of 900 plant species from more than 150 sites across China (Fig. 1), cementing its dominant status as a data center for phenological research in China. These phenology records have been contributed to examining the spatio-temporal patterns of plant phenological shifts (Dai et al., 2014; Ge et al., 2015), the environmental factors affecting plant phenology (Dai et al., 2013; Wang et al., 2020), and the development of phenology models in China (Tao et al., 2018). However, the spatial distribution of in-situ data is often uneven and limited, particularly at regional and global scales (Donnelly et al., 2022), with significant gaps over extended timescales. Advances in species-level phenology modeling offer a promising avenue to overcome these spatial and temporal constraints (Fu et al., 2020; Hufkens et al., 2018). In scenarios lacking of direct phenological observations, such models are invaluable for generating large-scale predictions, thereby filling in the missing data gaps in both space and time (Cleland et al., 2007; Wang et al., 2012). This modeling approach has been exemplified by the Extended Spring Indices (SI-x) model, which has produced detailed gridded maps delineating the first leaf and first bloom events for three woody plants across the contiguous United States with resolutions from 1° to 1 km (Ault et al., 2015; Izquierdo-Verdiguier et al., 2018). Adopting a similar strategy, it is feasible to extrapolate the CPON phenology observations across China, facilitating the integration and scaling up of this rich dataset to serve regional and national research needs.

In contrast to manual in-situ observations, satellite remote sensing facilitates expansive monitoring and mapping of land surface phenology (LSP) at a landscape scale, yielding more comprehensive phenological data (Studer et al., 2007). Over the past four decades, remote sensing technologies have witnessed substantial enhancements, leading to significant strides in both spatial and temporal resolution (Misra et al., 2020; Dronova and Taddeo, 2022). Currently, a variety of LSP products, based on vegetation indices like NDVI and EVI from diverse remote sensing sources, provide LSP data on regional and global scales with resolutions from 10 km down to 30 m (e.g., Li et al., 2019; Wu et al., 2021). The reliability of these LSP datasets is highly dependent on validation against ground phenology (GP) data derived from in-situ SP observations (Tian et al., 2021; Zhang et al., 2017), necessitating a seamless transition from individual (i.e., SP) to landscape (i.e., GP) level. Methods such as weighted averages and quantiles have proven their efficacy in this aggregation process from individual to community or landscape levels (Donnelly et al., 2022; Fitchett et al., 2015). For instance, the weighted average method has

删除[伊洛。]: To be helpful for

删除[伊洛。]: ons

删除[伊洛。]: , long-term, dependable plant phenology d

删除[伊洛。]: Presently,

删除[伊洛。]: manual

删除[伊洛。]: etc. Nevertheless,

删除[伊洛。]: between

删除[伊洛。]: different

删除[伊洛。]: precise phenological information

删除[伊洛。]: the

删除[伊洛。]: individual

删除[伊洛。]: a multitude of

删除[伊洛。]: incorporating

删除[伊洛。]: T

删除[伊洛。]: CPON has amassed

删除[伊洛。]: phenology

删除[伊洛。]: pertaining to more than

删除[伊洛。]: across over

删除[伊洛。]: throughout

删除[伊洛。]: as well as

删除[伊洛。]: phenology

删除[伊洛。]: observed

删除[伊洛。]: y

删除[伊洛。]: phenology

删除[伊洛。]: e

删除[伊洛。]: interpolating

删除[伊洛。]: been successfully applied to create gridded

删除[伊洛。]: 1: at a

66 been validated at the site scale through combined field and remote sensing studies to aggregate GP data from in-situ SP
67 observations, considering species abundance as weights (Liang et al., 2011). Recent studies have suggested that quantile
68 methods (e.g., 30th percentile) holds greater promise than the commonly used average methods at larger scales, as
69 demonstrated in Europe and the USA (Ye et al., 2022). Nevertheless, such methods have not yet been applied to aggregate
70 large-scale GP from SP data in China. This gap potentially limits the ground-truthing for LSP products and hampers a
71 comprehensive understanding of the spatial and temporal patterns of phenological shifts over the country.

72 In this study, we aimed to develop long-term, high-resolution SP and GP maps of China, spanning from 1951 to 2020
73 with a 0.1° resolution. This effort will produce spatially continuous, gridded phenology products that are notably missing in
74 the current Chinese context, yet are vital for diverse scientific and ecological applications. Drawing from the extensive
75 database of the CPON, we analyzed 24,552 in-situ phenology observations of 24 representative woody plants from 122 sites
76 over six decades. This analysis included three critical phenophases for each species: the first leaf date (FLD), first flower
77 date (FFD), and 100% leaf coloring date (LCD). In our methodology, we employed five species-level phenology models
78 with gridded meteorological data to simulate SP maps. To refine these maps for each plant species, we applied species
79 distribution maps as spatial filters. We further synthesized these SP maps into GP maps, utilizing weighted average and
80 quantile methods that incorporated the distribution probabilities of the species as weights. The SP maps underwent a
81 rigorous cross-validation process to ensure accuracy, while the GP maps' reliability was verified through comparative
82 analysis with existing LSP products. The contribution of this study is the introduction of a novel grid phenology dataset for
83 China. This dataset enhances the spectrum of available phenology data within the country and serves as an independent,
84 source for validating LSP products. Moreover, it is expected to significantly advance research on plant phenology and global
85 change by providing a more detailed portrayal of the spatiotemporal trends in plant phenology patterns.

86 2 Methods

87 2.1 Data acquisition and processing

88 2.1.1 Phenology observations

89 The in-situ phenology observations from 1963 to 2018 were obtained from the CPON. We selected 24 representative
90 woody plants species across 17 families (Table 1). These species are not only prevalent in China's forest ecosystems (Fang
91 et al., 2011), but also extensively recorded within CPON database. The longitudinal span of these observations covers 55
92 years across 122 sites, with a total of 24,552 individual records, covering a diverse spectrum of land cover, ecological, and
93 climatic conditions across China (Fig. 1). Each species in the study has a substantial representation in the dataset, with at
94 least 40 years of phenological data from a minimum of 13 distinct sites. We focused on three phenophases for each species:
95 spring FLD, spring FFD, and autumn LCD. To ensure the integrity of the dataset, we applied three-sigma limits, a statistical
96 filter that retains data within three standard deviations from the species' mean phenological dates (Pukelsheim, 1994).

删除[伊洛。]: on a

删除[伊洛。]: investigations

删除[伊洛。]: monitoring

删除[伊洛。]: ,

删除[伊洛。]: at the community or landscape levels

删除[伊洛。]: data

删除[伊洛。]: Some r

删除[伊洛。]: the

删除[伊洛。]: on a

删除[伊洛。]: there is no previous study endeavored to ...

删除[伊洛。]: for

删除[伊洛。]: ing

删除[伊洛。]: ,

删除[伊洛。]: which may

删除[伊洛。]: constrain the availability of ground valida ...

删除[伊洛。]: o-

删除[伊洛。]: characteristics

删除[伊洛。]: changes

删除[伊洛。]: spanning 1951-2020

删除[伊洛。]: ,

删除[伊洛。]: W

删除[伊洛。]: the past

删除[伊洛。]: from CPON

删除[伊洛。]: T

删除[伊洛。]: , namely

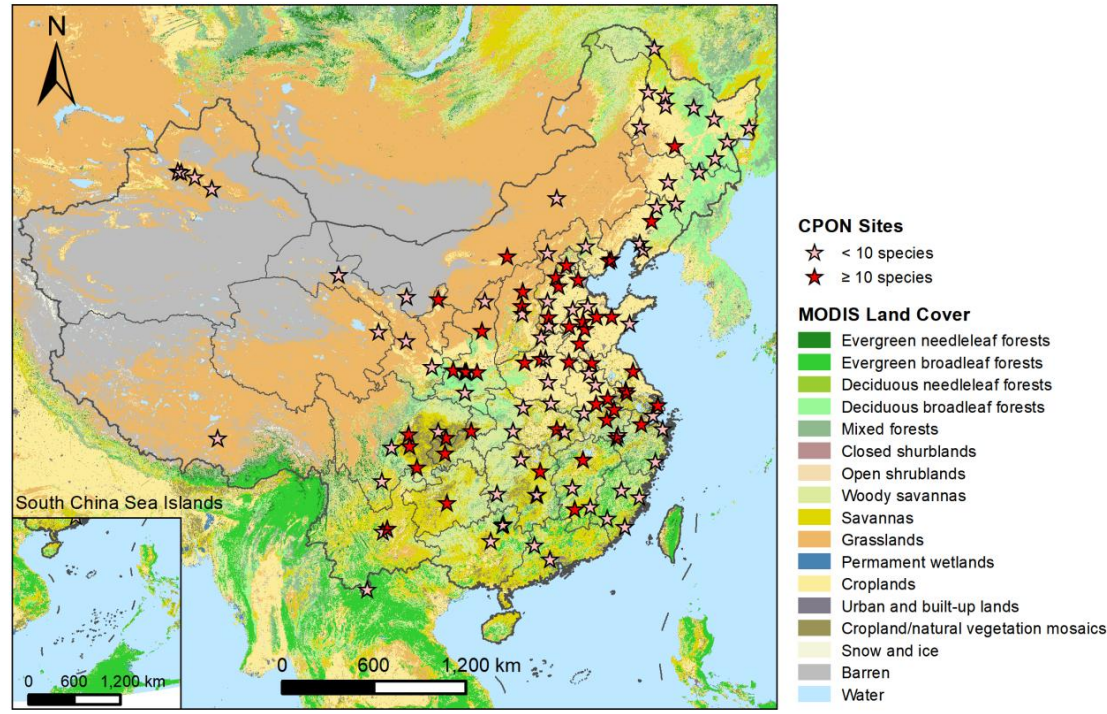
删除[伊洛。]: , were included for each species

删除[伊洛。]: W

删除[伊洛。]: 1. and produce

97 Outliers that fell beyond these thresholds were excluded, as they constitute less than 1% of the data points on a standard
 98 normal distribution, ensuring a robust and reliable dataset for analysis.

删除[伊洛。]: o
 删除[伊洛。]: all
 删除[伊洛。]: curve



99
 100 **Figure 1:** Geographic distribution of CPON sites (n = 122) included in the phenology dataset across China. Sites with less
 101 than 10 recorded species are marked with pink asterisks, while sites with more than 10 recorded species are marked with red
 102 asterisks. Note that the markings on the map of several adjacent sites may overlap each other. The background map shows
 103 the IGBP land cover type from the MODIS Land Cover product (Friedl and Sulla-Menashe, 2022).

104
 105 **Table 1:** List of 24 species of woody plants from 17 families in China. Number of records represents the total number of
 106 three phenophases (FLD, FFD and LCD) of all sites and all years for each species.

No.	Species	Family	Life form	Number of sites	Number of years	Number of records
1	<i>Ginkgo biloba</i>	Ginkgoaceae	Tree	45	49	1110
2	<i>Metasequoia glyptostroboides</i>	Cupressaceae	Tree	37	47	860
3	<i>Magnolia denudata</i>	Magnoliaceae	Tree	42	47	980
4	<i>Salix babylonica</i>	Salicaceae	Tree	65	42	1526

5	<i>Populus × canadensis</i>	Salicaceae	Tree	43	51	954
6	<i>Robinia pseudoacacia</i>	Fabaceae	Tree	54	45	1757
7	<i>Albizia julibrissin</i>	Fabaceae	Tree	36	47	984
8	<i>Cercis chinensis</i>	Fabaceae	Shrub	52	49	1207
9	<i>Prunus armeniaca</i>	Rosaceae	Tree	46	45	950
10	<i>Ulmus pumila</i>	Ulmaceae	Tree	60	44	1428
11	<i>Morus alba</i>	Moraceae	Tree	50	50	1071
12	<i>Broussonetia papyrifera</i>	Moraceae	Tree	41	43	1103
13	<i>Quercus acutissima</i>	Fagaceae	Tree	17	40	292
14	<i>Pterocarya stenoptera</i>	Juglandaceae	Tree	29	46	936
15	<i>Juglans regia</i>	Juglandaceae	Tree	50	47	816
16	<i>Betula platyphylla</i>	Betulaceae	Tree	13	43	369
17	<i>Acer pictum</i> subsp. <i>mono</i>	Sapindaceae	Tree	18	46	492
18	<i>Ailanthus altissima</i>	Simaroubaceae	Tree	34	47	873
19	<i>Melia azedarach</i>	Meliaceae	Tree	61	46	1410
20	<i>Firmiana simplex</i>	Malvaceae	Tree	57	48	1403
21	<i>Hibiscus syriacus</i>	Malvaceae	Shrub	58	47	1096
22	<i>Fraxinus chinensis</i>	Oleaceae	Tree	23	40	505
23	<i>Syringa oblata</i>	Oleaceae	Shrub	50	51	1163
24	<i>Paulownia fortunei</i>	Paulowniaceae	Tree	49	48	1267
Total		-	-	122	55	24552

107

108 2.1.2 Climate data

109 The daily mean temperature (T) data spanning from 1950 to 2020 were sourced from two distinct repositories: (1) Site-
110 specific temperature (Site T) was retrieved from the China Meteorological Data Service Center (CMDSC,
111 https://data.cma.cn/). This dataset was primarily utilized for parameterizing the phenology models. (2) Gridded temperature
112 (Grid T) was derived from the ERA5-Land climate reanalysis datasets (Muñoz Sabater, 2019; Muñoz-Sabater et al., 2021).
113 available through the Copernicus Climate Change Service (C3S, https://cds.climate.copernicus.eu/). Grid T was employed
114 for phenology simulation and upscaling processes, with a fine spatial resolution of 0.1°, approximately equating to 10 km,

删除[伊洛。]: -

删除[伊洛。]: climate observations in

删除[伊洛。]: e

删除[伊洛。]: from

删除[伊洛。]: at

删除[伊洛。]:)

115 To obtain daily grid T values, we computed the average from hourly temperature data recorded at four distinct times of the
116 day (4:00, 10:00, 16:00, 22:00).

117 The current bioclimatic variables (BIOCLIM+) were obtained from Climatologies at High Resolution for the Earth
118 Land Surface Areas (CHELSA, <https://chelsa-climate.org/>) to determine the species distribution (Brun et al., 2022a, b).
119 These variables encapsulate the average ecological and climatic conditions for the period 1981-2010, boasting a high
120 resolution of 0.0083°. From the available bioclimatic data, we extracted both the traditional set of 19 bioclimatic layers
121 (Bio1-Bio19) and an additional set of 50 layers. To mitigate the effects of autocorrelation among these bioclimatic variables,
122 we computed the correlation coefficient between each pair of layer. Variables exhibiting a correlation coefficient above 0.8
123 relative to preceding layers were omitted to prevent redundancy. Consequently, a subset of 12 bioclimatic layers was
124 selected for inclusion as the environmental variables within the species distribution models (detailed in Table S1). These
125 selected layers were then resampled to a 0.1° resolution to ensure consistency with the resolution of the grid T data.

126 2.1.3 Forest and species distribution data

127 The forest distribution map of China was sourced from the dataset of “Annual Dynamics of Global Land Cover and its
128 Long-term Changes from 1982 to 2015” dataset (Liu et al., 2020). To discern forested regions, we reclassified the annual
129 land cover (LC) layers into ‘forest’ and ‘non-forest’ categories. We then determined the duration of forest cover by summing
130 the annual layers, and pixels representing at least one year of forest cover were identified as forest distribution areas. For
131 forest type categorization, we employed the widely recognized International Geosphere-Biosphere Program (IGBP)
132 classification system from the MODIS Land Cover Type (MCD12C1) Version 6.1 data product (Friedl and Sulla-Menashe,
133 2022). In our classification scheme, we combined evergreen needleleaf forest (class 1) and evergreen broadleaf forest (class
134 2) to delineate evergreen forest category. Similarly, deciduous needleleaf (class 3) and deciduous broadleaf forest (class 4)
135 were amalgamated into deciduous forest category. The mixed forest (class 5) category was retained as is. To achieve a
136 consistent spatial resolution across our datasets, both the forest distribution map and forest type map were resampled from
137 their original 0.05° resolution to a 0.1° resolution using the majority method, to match the resolution of the grid T data.

138 The county-level species distribution maps were sourced from the comprehensive Database of China's Woody Plants
139 (Fang et al., 2011). This authoritative database consolidates distribution data from an exhaustive suite of national, provincial,
140 and regional floristic surveys and inventory reports published in China up to 2009 (Cai et al., 2021). Additionally, we
141 obtained 4,371 occurrence records for 24 selected woody plant species from the Global Biodiversity Information Facility
142 (GBIF, 2022; <https://www.gbif.org/>), which were subsequently utilized as the occurrence data inputs for species distribution
143 modeling (detailed in Table S2). To ensure the reliability of our data, we included only those occurrence records that had
144 location coordinate with an uncertainty of less than 2,000 meters. Moreover, the dataset was meticulously cleansed to
145 eliminate any duplicate records, thereby enhancing the robustness of the species distribution models employed in our
146 analysis.

删除[伊洛。]: H

删除[伊洛。]: to derive the daily grid T

删除[伊洛。]: variables

删除[伊洛。]: BIOCLIM+

删除[伊洛。]: W

删除[伊洛。]: bioclimatic

删除[伊洛。]: in China

删除[伊洛。]: W

删除[伊洛。]: every two

删除[伊洛。]: s

删除[伊洛。]: to reduce the impact of autocorrelation an ...

删除[伊洛。]: and then excluded the layers with

删除[伊洛。]: greater than

删除[伊洛。]: with the previous

删除[伊洛。]: As a result

删除[伊洛。]: ere

删除[伊洛。]: retained

删除[伊洛。]: for

删除[伊洛。]: match

删除[伊洛。]: Each year's

删除[伊洛。]: were reclassified

删除[伊洛。]: as

删除[伊洛。]: ,

删除[伊洛。]: and

删除[伊洛。]: the number of years

删除[伊洛。]: was obtained

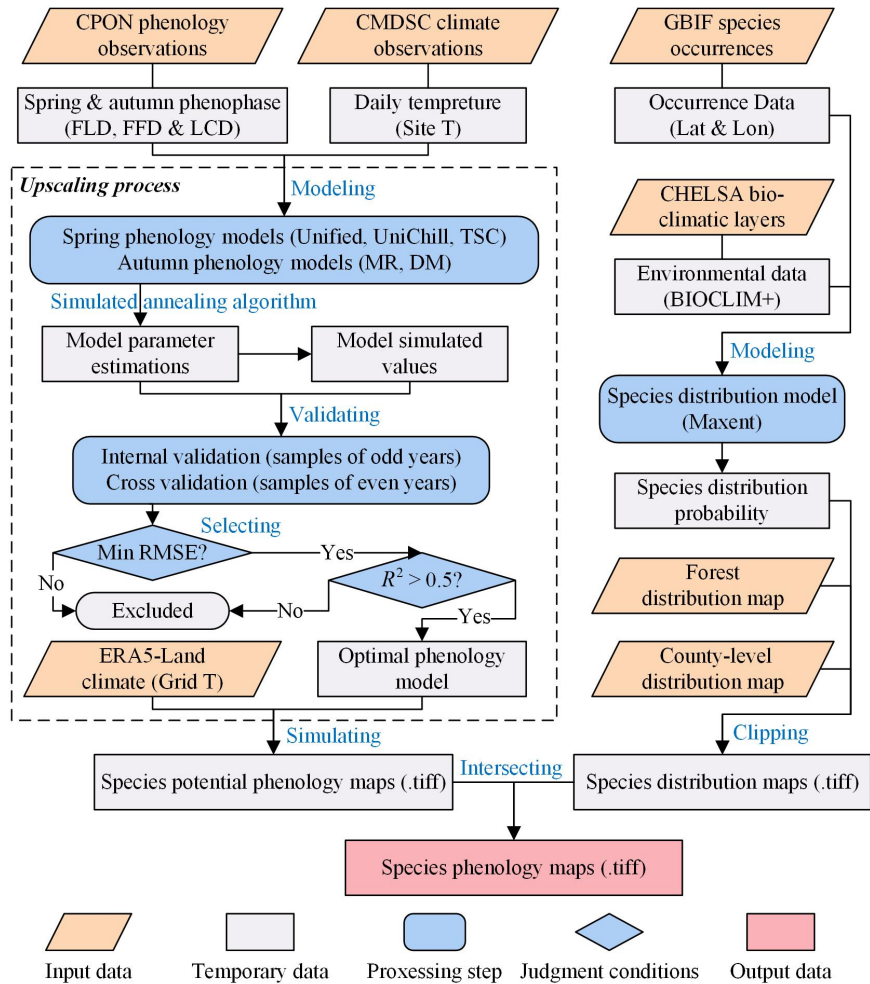
删除[伊洛。]: add

删除[伊洛。]: all

147 **2.2 Generating species phenology maps using a model-based upscaling method**

148 The generation of **SP** maps involves two major processes: (1) **generating species potential phenology maps**, and (2)
 149 **generating species distribution maps**. The **definitive** SP maps **emerged from the spatial intersection of** these two **distinct map**
 150 **types, effectively overlaying the potential phenology with the actual distribution to pinpoint precise phenological patterns.**

151 The workflow for the processes is shown in Fig. 2.



删除[伊洛。]: species phenology
 删除[伊洛。]: G
 删除[伊洛。]: G
 删除[伊洛。]: final
 删除[伊洛。]: were obtained by
 删除[伊洛。]: s
 删除[伊洛。]: patially intersecting
 删除[伊洛。]: s

152
 153
 154
 155
 156

Figure 2: The workflow of generating SP maps using a model-based upscaling method, which involves two major processes: (1) Generating species potential phenology maps, and (2) Generating species distribution maps. The words in blue color represent the key processes of data generation. “.tiff” indicates the GeoTIFF format of the grid phenology or distribution maps.

157 2.2.1 Species potential phenology maps

158 In the first process, we **employed** a model-based upscaling method to **transform** in-situ phenology observations into
159 **gridded** phenology maps. Phenology models were **constructed utilizing** the phenophases (i.e., FLD, FFD, LCD), **recorded by**
160 **the** CPON, **in conjunction with the** site T from **the** CMDSC climate observations. For each species **under study**, we
161 **developed a suite of phenology models to the respective seasonal phases.** **Three models were designated for** spring
162 phenology: the Unichill, Unified (Chuine, 2000) and temporal-spatial coupling (TSC) models (Ge et al., 2014). **And two**
163 **models were designated for** autumn phenology: the multiple regression (MR) (Estrella and Menzel, 2006) and temperature-
164 photoperiod (TP) models (Delpierre et al., 2009). The details of the **modeling** formulae **and their respective parameters are**
165 **elaborated upon**, in Appendix S1. **The modeling strategy involved a cross-validation approach, where data** from odd years
166 were used for **model training, while data** from even years were **set aside for model validation purposes.** **The estimation of all**
167 model parameters **was executed via** the simulated annealing algorithm (Chuine et al., 1998), **ensuring a robust optimization**
168 **process for the phenology models.**

169 For model validation, the models' root mean square error (RMSE) and goodness of fit (R^2) were calculated between the
170 model **predicted** values and **the** original **observed** values. **We conducted an** internal validation, **using the data** from odd years
171 to evaluate the **models' fitting efficacy.** **On the other hand, we conducted a** cross validation **was on data** from even years to
172 evaluate **the models' capability to simulate and extrapolate phenology data beyond the sample used for model development.**
173 The optimal phenology model for each species was **determined as the one with** the smallest RMSE **during the cross-**
174 **validation process** and **an R^2 exceeding 0.5 (or 0.3 for LCD) during both validation processes.** **Species for which** no model
175 met these **predefined criteria** were omitted from the subsequent generation of SP and GP maps.

176 **To simulate** SP maps, **we input** daily grid T data from ERA5-Land climate reanalysis, into the **previously determined**
177 optimal phenology models **for each species.** **The simulation was conducted on a** pixel-by-pixel basis, **enabling the**
178 **interpolation and upscaling of** phenology observations from **discrete** sites, to a **comprehensive** gridded phenology maps
179 (Chuine et al., 2000). **It is important to note, however, that the availability of** grid T data, **allows for the simulation of,** species
180 phenology, even **in areas lacking observed** species distribution. Therefore, we **refer to the resultant maps**, as species potential
181 phenology maps. **This distinction emphasizes that while the simulated values represent potential phenological events based**
182 **on climatic variables, they should not be misconstrued as actual observed values in regions where the species does not exist,**

183 2.1.2 Species distribution maps

184 In the second process, species distribution maps **were generated by integrating** species distribution models **with** county-
185 level species distribution data. **For each species, we constructed** models, using **the** Maximum Entropy Species Distribution
186 Modelling (Maxent; Phillips et al., 2006) version.3.4.4. Maxent **is a widely utilized tool in species distribution modeling due**
187 **to its efficacy in** estimating a species' **distributional range** by finding the **distribution pattern with** maximum entropy (i.e.,
188 closest to the uniform), **Maxent models the likelihood of species presence across geographical grids, assigning a predicted**

删除[伊洛。]: from

删除[伊洛。]: phenology observations

删除[伊洛。]: built t

删除[伊洛。]: models

删除[伊洛。]: ,

删除[伊洛。]: a

删除[伊洛。]: models

删除[伊洛。]: are described

删除[伊洛。]: For each model,

删除[伊洛。]: samples

删除[伊洛。]: phenology modeling

删除[伊洛。]: and samples

删除[伊洛。]: reserved for cross validation on the model

删除[伊洛。]: A

删除[伊洛。]: were

删除[伊洛。]: estimated using

删除[伊洛。]: I

删除[伊洛。]: was conducted

删除[伊洛。]: on samples

删除[伊洛。]: fitting effect of the model

删除[伊洛。]: ,

删除[伊洛。]: and

删除[伊洛。]: conducted

删除[伊洛。]: samples

删除[伊洛。]: the simulation and extrapolation effect of

删除[伊洛。]: in cross validation

删除[伊洛。]: greater than

删除[伊洛。]: 1. If

189 probability of occurrence to each grid cell. To configure the Maxent model, we utilized occurrence data from the GBIF
190 database, paired with environmental data inputs from the 12 bioclimatic layers provided by BIOCLIM+. In the model
191 parameter settings, both linear and quadratic feature types were used to capture the relationship between species presence
192 and environmental variables. Additionally, to validate the model and assess its predictive performance, we employed a 5-
193 fold cross validation method.

194 To evaluate the accuracy of the Maxent species distribution models, we applied the receiver operating characteristic
195 (ROC) curve analysis. The integral of the ROC curve, referred to as the area under the curve (AUC), serves as a quantitative
196 measure of the model's prediction accuracy. (Fielding and Bell, 1997). An AUC value approaching 1.0 is indicative of a
197 model with high predictive accuracy. In our study, the Maxent models demonstrated robust predictive power, with an
198 average test AUC of 0.845, and a standard deviation of 0.043 across the different species (Table S2).

199 2.3 Generating ground phenology maps using weighted average and weighted quantile methods

200 In our study, we aggregated individual-level SP maps into landscape-level GP maps using four aggregation methods: (1)
201 weighted average (mean); (2) weighted median (pct50); (3) weighted 20th percentile (pct20) for spring phenology or
202 weighted 80th percentile (pct80) for autumn phenology; (4) weighted 10th percentile (pct10) for spring phenology or
203 weighted 90th percentile (pct90) for autumn phenology. Previous studies typically utilized species abundance as weights for
204 aggregation at a local scale, but obtaining such data at the regional scale proves challenging. Therefore, we replaced species
205 abundance with species distribution probability as aggregation weight for each species. This assumption stems from the
206 positive correlation between species distribution and abundance (Brown, 1984), indicating that species tend to exhibit higher
207 abundance in the core of their geographic range (Sagarin and Gaines, 2002). The aggregation techniques applied in this
208 study (e.g., pct50, pct20\80 and pct10\90) are analogous to the methods used for extracting LSP from remote sensing data
209 (e.g., midpoint, dynamic threshold and maximum curvature). The procedures followed in the generation of GP maps are
210 illustrated in Fig. 3.

211

删除[伊洛。]: It expresses a probability distribution whe

删除[伊洛。]: build

删除[伊洛。]: species location records

删除[伊洛。]: were used as occurrence data input

删除[伊洛。]: and

删除[伊洛。]: from

删除[伊洛。]: were used as the environmental data input

删除[伊洛。]: and

删除[伊洛。]: was used as the replicated run type

删除[伊洛。]: method was used to test the accuracy of tl

删除[伊洛。]: value

删除[伊洛。]: as an indicator

删除[伊洛。]: of the model

删除[伊洛。]: The closer the

删除[伊洛。]: , the more accurate the prediction result of

删除[伊洛。]: The

删除[伊洛。]: for different species

删除[伊洛。]: was

删除[伊洛。]: ,

删除[伊洛。]: with

删除[伊洛。]: W

删除[伊洛。]: four methods

删除[伊洛。]: aggregate from individual-level SP maps to

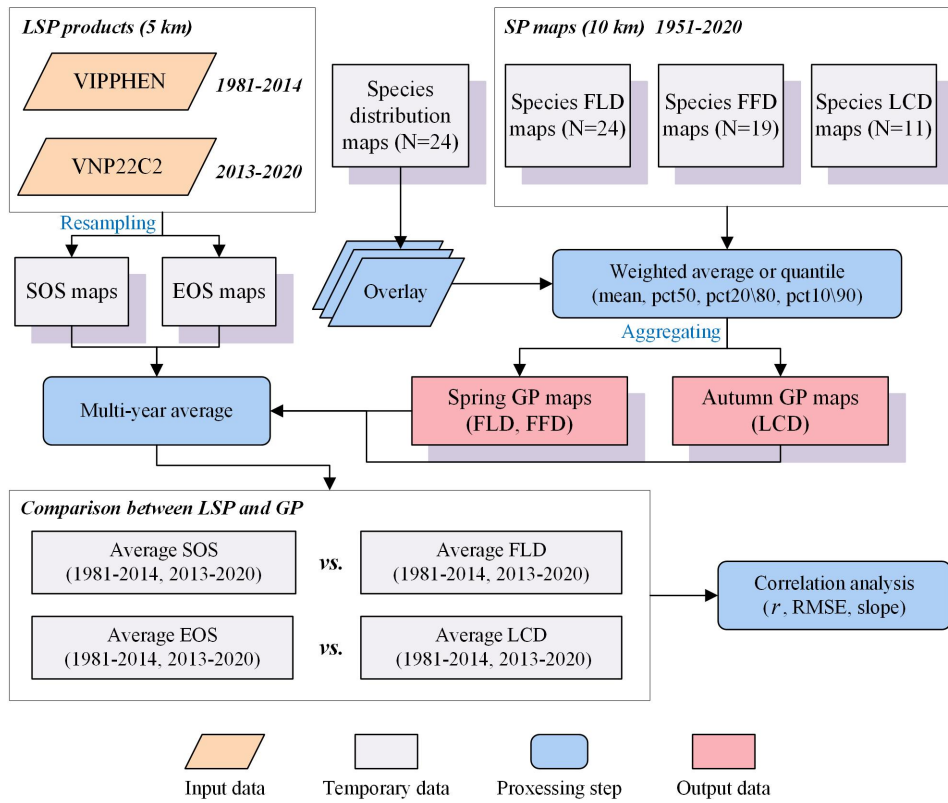
删除[伊洛。]: aggregation

删除[伊洛。]: the

删除[伊洛。]: it is difficult to

删除[伊洛。]: instead of species abundance

删除[伊洛。]: 1: is based on



212

213 **Figure 3:** The workflow of generating GP maps from SP maps, and comparing GP maps with two LSP products. The words
 214 in blue color represent the key processes of data generation.

215

216 For n species, the phenological data were first arranged in ascending order. The SP of each species is y_i ($i =$
 217 $1, 2, \dots, n$), and the distribution probability of each species is p_i ($i = 1, 2, \dots, n$). Then, the aggregated GP (Y_{mean} and Y_{pct}
 218 ($x\%$)) was calculated according to the following formulas:

$$219 \quad \omega_i = \frac{p_i}{\sum_{i=1}^n p_i} \quad (1)$$

$$220 \quad W_j = \sum_{i=1}^j \omega_i, j = 1, 2, \dots, n \quad (2)$$

$$221 \quad Y_{mean} = \sum_{i=1}^n \omega_i \times y_i \quad (3)$$

$$222 \quad Y_{pct} = \begin{cases} y_1, & \text{if } W_1 > x \\ (y_j - y_{j-1}) \times \frac{x - W_{j-1}}{\omega_j}, & \text{if } W_j > x, W_{j-1} < x \\ y_n, & \text{if } W_{n-1} < x \end{cases} \quad (4)$$

where ω_i is a weight to each species, W_j is the cumulative weight from the 1st to the j -th species, $x\%$ is the percentile tag which takes values from 10%, 20%, 50%, 80% and 90%. These calculations enable the construction of aggregated GP maps by combining species phenology maps with species distribution maps and weighting them by species distribution probability.

To evaluate the data quality and reliability of the aggregated GP maps, we undertook a comparative analysis with two established LSP products derived from remote sensing data: (1) VIPPHEN NDVI dataset (1981-2014), utilized the midpoint method to extract the start of season (SOS) and the end of season (EOS) from the AVHRR data (Didan and Barreto, 2016); (2) VNP22C2 dataset product (2013-2020), utilized the maximum curvature method to derive SOS and EOS from the MODIS data (Zhang et al., 2020). To align the spatial resolution of these datasets with our GP maps, we resampled both LSP products from 5 km to 0.1° using the average method. Subsequently, we conducted a correlation analysis to assess the consistency between our GP data and the LSP products, specifically comparing the FLD with SOS for the spring, and the LCD with EOS for the autumn. The comparison involved averaging the LSP and GP maps across two distinct periods: 1981-2014 and 2013-2020. The statistical measures calculated for this assessment included the Pearson correlation coefficient (r), RMSE, and linear regression slope between GP and LSP across different forest types (Table S3).

3 Results and discussion

The dataset encompasses two distinct types of phenology maps over China: (1) Annual SP maps for 24 woody plants species, constructed using the model-based upscaling method; (2) Annual GP maps for forest vegetation, generated by four aggregation methods, accompanied by quality assurance (QA) maps. These maps detail the phenological events of FLD, FFD in spring, and LCD in autumn, spanning from 1951 to 2020, with a spatial resolution of 0.1° and a temporal resolution of 1 day. Each phenology map is stored as a 16-bit signed integer, within GeoTIFF file format, comprising a two-dimension raster (641 row \times 361 column). The phenology data are expressed in Julian Day of the year (DOY), indicating the elapsed number of days from January 1st to the occurrence of phenological event. The dataset's valid DOY values range from 1 to 366, while null values are denoted by -1.

3.1 Simulation and validation of species phenology maps

The SP maps of FLD (24 species), FFD (19 species), and LCD (12 species) were generated by applying the optimal phenology models. Here, we present the results of the SP maps for four emblematic woody species (Fig. 4), including ginkgo (*Ginkgo biloba*), willow (*Salix babylonica*), elm (*Ulmus pumila*), and lilac (*Syringa oblata*). These maps have been refined using species distribution maps to ensure that the simulated phenologies were relevant only to areas where the species are known to exist. The presented maps illustrate a clear spatial pattern in the timing of phenophases correlated with latitude. Specifically, the onset of spring event such as FLD and FFD for these species is markedly delayed with increasing latitude. Conversely, the autumn LCD occurs earlier as the latitude increases. While these spatial patterns are consistent across

删除[伊洛。]: W

删除[伊洛。]: the

删除[伊洛。]: of

删除[伊洛。]: first

删除[伊洛。]:

删除[伊洛。]: formulas

删除[伊洛。]: the

删除[伊洛。]: the

删除[伊洛。]: the

删除[伊洛。]: the

删除[伊洛。]: Finally, t

删除[伊洛。]: ,

删除[伊洛。]: in this study were

删除[伊洛。]: in previous studies

删除[伊洛。]: product

删除[伊洛。]: which used

删除[伊洛。]: B

删除[伊洛。]: were resampled

删除[伊洛。]:

删除[伊洛。]: by

删除[伊洛。]: to match the spatial resolution of GP maps

删除[伊洛。]: The LSP and GP maps were averaged in t...

删除[伊洛。]: was conducted

删除[伊洛。]: between

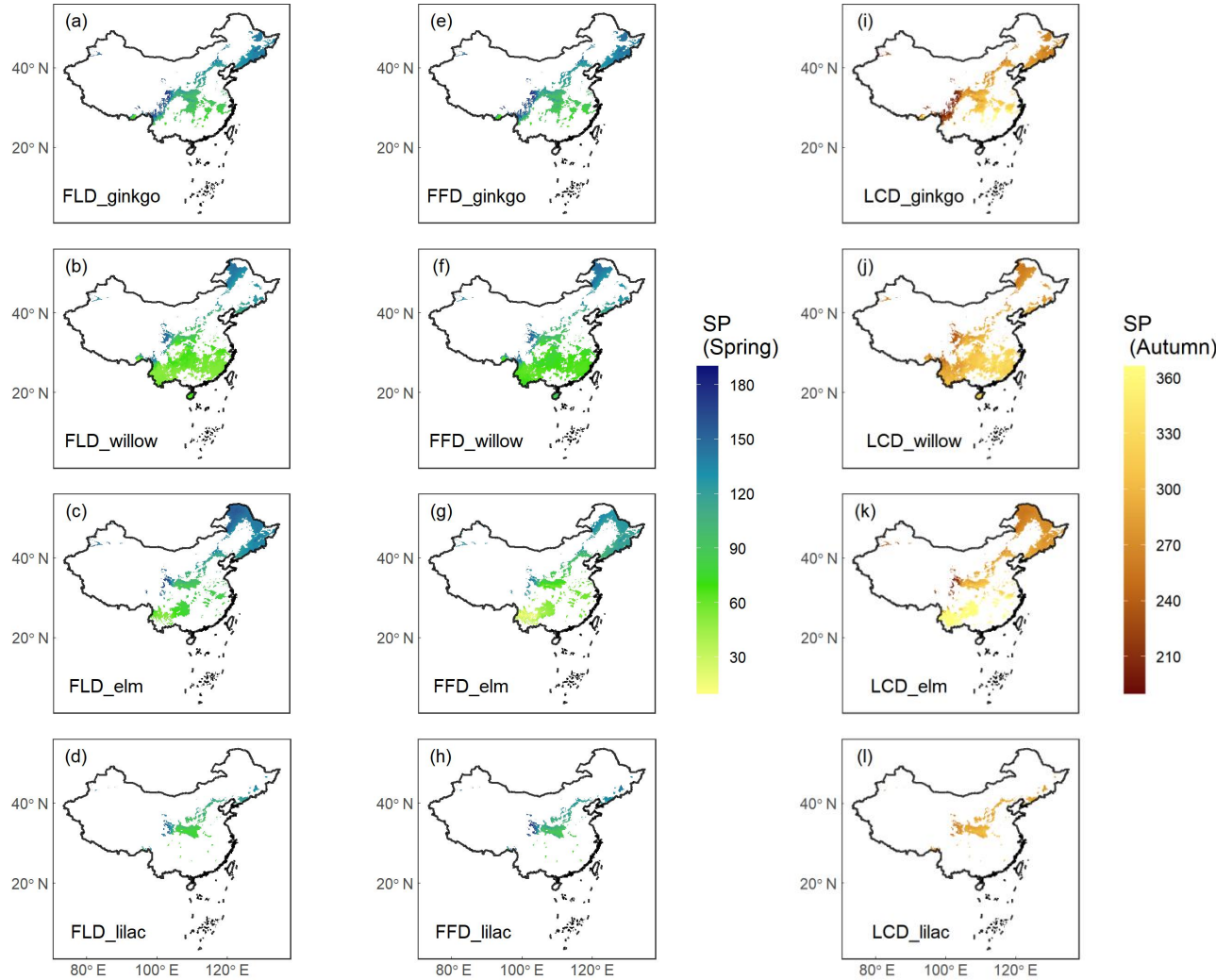
删除[伊洛。]: and

删除[伊洛。]: in

删除[伊洛。]: between

删除[伊洛。]: 1. and

254 species, there are notable temporal differences at the same latitudes. For example, at lower latitudes, the elm exhibits an
 255 earlier FFD in spring and a later LCD in autumn compared to the other species. Phenophases for some species were not
 256 included in the simulation, because the suboptimal explanatory power of their phenology models, e.g., $R^2 < 0.5$ for spring
 257 FFD, and $R^2 < 0.3$ for autumn LCD.
 258



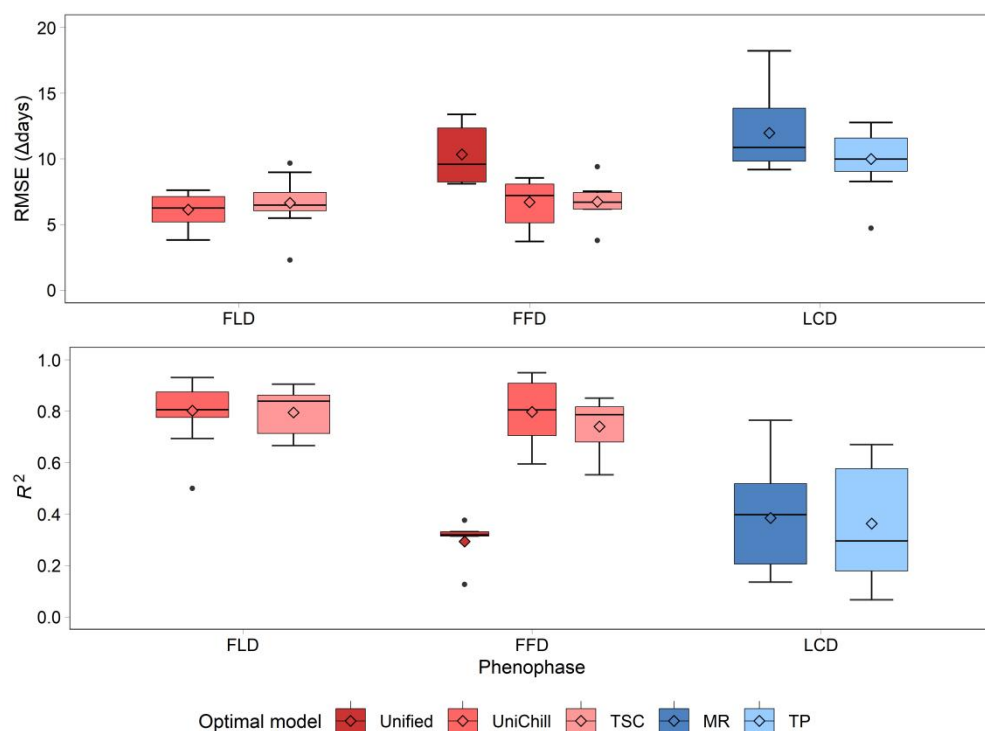
删除[伊洛。]: the phenophases of different species show distinct
 删除[伊洛。]: ;
 删除[伊洛。]: f
 删除[伊洛。]: has significantly
 删除[伊洛。]: FFD
 删除[伊洛。]: LCD than
 删除[伊洛。]: of
 删除[伊洛。]: simulated
 删除[伊洛。]: the R^2 of their optimal models was too small

259
 260 **Figure 4:** Species phenology (SP) maps of four typical woody species averaged from 1951 to 2020. Columns 1-2 show the
 261 spring phenophases (FLD and FFD), and Column 3 shows the autumn phenophase (LCD). Each row represents a species
 262 from ginkgo (*Ginkgo biloba*), willow (*Salix babylonica*), elm (*Ulmus pumila*), and lilac (*Syringa oblata*). The unit of
 263 phenology data is the Julian Day of year (DOY) from January 1st.
 264

No.	Species	FLD			FFD			LCD		
		Optimal model	RMSE	R^2	Optimal model	RMSE	R^2	Optimal model	RMSE	R^2
1	<i>Ginkgo biloba</i>	TSC	7.30	0.669	TSC	7.53	0.553	DM	12.54	0.401
2	<i>Metasequoia glyptostroboides</i>	TSC	6.10	0.687	Unified	9.59	0.126	DM	9.99	0.295
3	<i>Magnolia denudata</i>	UniChill	6.47	0.781	TSC	7.33	0.576	DM	9.31	0.284
4	<i>Salix babylonica</i>	TSC	8.97	0.854	TSC	9.40	0.787	MR	18.23	0.380
5	<i>Populus × canadensis</i>	UniChill	5.94	0.808	UniChill	6.14	0.728	MR	9.45	0.139
6	<i>Robinia pseudoacacia</i>	TSC	5.47	0.863	TSC	6.18	0.785	DM	11.74	0.297
7	<i>Albizia julibrissin</i>	UniChill	7.48	0.500	Unified	8.23	0.376	MR	9.18	0.567
8	<i>Cercis chinensis</i>	TSC	7.90	0.723	UniChill	7.39	0.751	DM	9.09	0.175
9	<i>Prunus armeniaca</i>	TSC	6.05	0.865	UniChill	4.78	0.929	MR	14.52	0.191
10	<i>Ulmus pumila</i>	UniChill	5.09	0.901	UniChill	8.38	0.862	DM	11.16	0.654
11	<i>Morus alba</i>	TSC	6.70	0.905	UniChill	7.99	0.860	DM	9.04	0.175
12	<i>Broussonetia papyrifera</i>	UniChill	7.60	0.804	TSC	6.18	0.821	DM	9.97	0.615
13	<i>Quercus acutissima</i>	UniChill	6.73	0.931	UniChill	5.12	0.950	MR	14.35	0.765
14	<i>Pterocarya stenoptera</i>	UniChill	7.52	0.804	UniChill	7.89	0.710	MR	11.57	0.415
15	<i>Juglans regia</i>	TSC	6.04	0.739	UniChill	8.54	0.595	DM	8.41	0.141
16	<i>Betula platyphylla</i>	UniChill	3.80	0.915	UniChill	3.70	0.906	DM	8.27	0.655
17	<i>Acer pictum</i> subsp. <i>mono</i>	TSC	2.29	0.894	TSC	3.78	0.814	DM	4.71	0.670
18	<i>Ailanthus altissima</i>	UniChill	5.22	0.867	UniChill	8.34	0.664	DM	10.39	0.066
19	<i>Melia azedarach</i>	TSC	6.81	0.828	TSC	6.70	0.851	MR	10.19	0.135
20	<i>Firmiana simplex</i>	UniChill	6.02	0.694	Unified	8.10	0.314	DM	12.30	0.190
21	<i>Hibiscus syriacus</i>	TSC	9.66	0.666	Unified	13.38	0.331	DM	12.76	0.464
22	<i>Fraxinus chinensis</i>	TSC	6.25	0.852	Unified	12.35	0.319	MR	9.76	0.533
23	<i>Syringa oblata</i>	UniChill	7.01	0.864	UniChill	5.11	0.920	MR	12.36	0.475

24	<i>Paulownia fortunei</i>	UniChill	4.63	0.762	UniChill	7.02	0.693	MR	10.01	0.250
----	---------------------------	----------	------	-------	----------	------	-------	----	-------	-------

267 The effectiveness of the simulated SP maps was evaluated by cross-validation on the optimal phenology models (Table
268 2). The results showed that spring phenology yielded significantly more accurate simulations than autumn phenology (Fig.
269 5). Quantitatively, the RMSE for the optimal model of FLD (6.38 days) and FFD (7.46 days) in spring were significantly
270 smaller than that of LCD (10.80 days) in autumn. Correspondingly, the R^2 for spring FLD (0.799) and FFD (0.676) was
271 significantly higher compared to autumn LCD (0.372). When comparing the simulation effects of FLD and FFD in spring,
272 no significant difference was observed. Among the optimal spring phenology models, the FFD simulations derived from the
273 UniChill and TSC models demonstrated significantly better performance than those from the Unified model. Conversely, for
274 autumn phenology, the simulation effects LCD were comparable between the MR and TP models.



277 **Figure 5:** The RMSE (a) and R^2 (b) of cross-validation on the optimal phenology models for 24 woody species. Each model
278 is represented by a different color, with warm colors for three spring phenology models (Unified, UniChill, TSC), and cool
279 colors for two autumn phenology models (MR, TP). The model with the smallest RMSE was selected as the optimal model
280 for each species. The horizontal line represents the median value, the diamond mark represents the mean value, and the dot
281 mark represents the outlier in the boxplot.

删除[伊洛。]: simulation effects of
删除[伊洛。]: species phenology
删除[伊洛。]: ere
删除[伊洛。]: the simulation effects of
删除[伊洛。]: were
删除[伊洛。]: better
删除[伊洛。]: that of
删除[伊洛。]: of
删除[伊洛。]: of
删除[伊洛。]: the optimal model of
删除[伊洛。]: in spring
删除[伊洛。]: ere
删除[伊洛。]: in autumn
删除[伊洛。]: However, there was
删除[伊洛。]: between spring FLD and FFD simulation effects
删除[伊洛。]: simulation effects of
删除[伊洛。]: were
删除[伊洛。]: .
删除[伊洛。]: But
删除[伊洛。]: in
删除[伊洛。]: LCD
删除[伊洛。]: a
删除[伊洛。]: similar for

283 **3.2 Aggregation of ground phenology maps**

284 The results of GP maps generated by four ~~distinct~~ aggregation methods (mean, pct50, pct20\80, pct10\90) ~~exhibited~~
285 similar spatial patterns (Fig. 6). ~~These maps demonstrate a~~ consistent ~~pattern of phenological~~ variation ~~in relation to both~~
286 latitude ~~and~~ altitude. ~~Specifically, with~~ increasing latitude or altitude, spring GP (FLD and FFD) ~~occurred progressively~~
287 later, ~~while~~ autumn GP (LCD) ~~occurred~~ earlier. ~~When comparing the various~~ aggregation methods, the GP maps aggregated
288 ~~by~~ the mean and pct50 methods ~~showed a high degree of consistency~~, with r being 0.992. ~~In contrast~~, the GP maps
289 aggregated ~~by~~ the pct20\80 and pct10\90 methods ~~exhibited~~ slightly ~~more spatial variability and were less correlated with~~ the
290 former ~~methods~~, with r being 0.968 and 0.949, ~~respectively~~. The ~~remarkable~~ consistency between the ~~maps aggregated~~
291 ~~through~~ mean and pct50 ~~methods suggests~~ that both the weighted mean ~~and~~ weighted quantile ~~approaches are~~ robust ~~and~~
292 ~~reliable~~ for the aggregation of GP.

293

删除[伊洛。]: different

删除[伊洛。]: showed

删除[伊洛。]: ,

删除[伊洛。]: i.e., the

删除[伊洛。]: along

删除[伊洛。]: or

删除[伊洛。]: W

删除[伊洛。]: the

删除[伊洛。]: e of

删除[伊洛。]: the

删除[伊洛。]: became

删除[伊洛。]: and the

删除[伊洛。]: became

删除[伊洛。]: For different

删除[伊洛。]: from

删除[伊洛。]: were highly consistent

删除[伊洛。]: ;

删除[伊洛。]: while

删除[伊洛。]: from

删除[伊洛。]: were

删除[伊洛。]: different from

删除[伊洛。]: two

删除[伊洛。]: and showed larger spatial variation than th ...

删除[伊洛。]: high

删除[伊洛。]: maps indicated

删除[伊洛。]: method

删除[伊洛。]: method

删除[伊洛。]: were

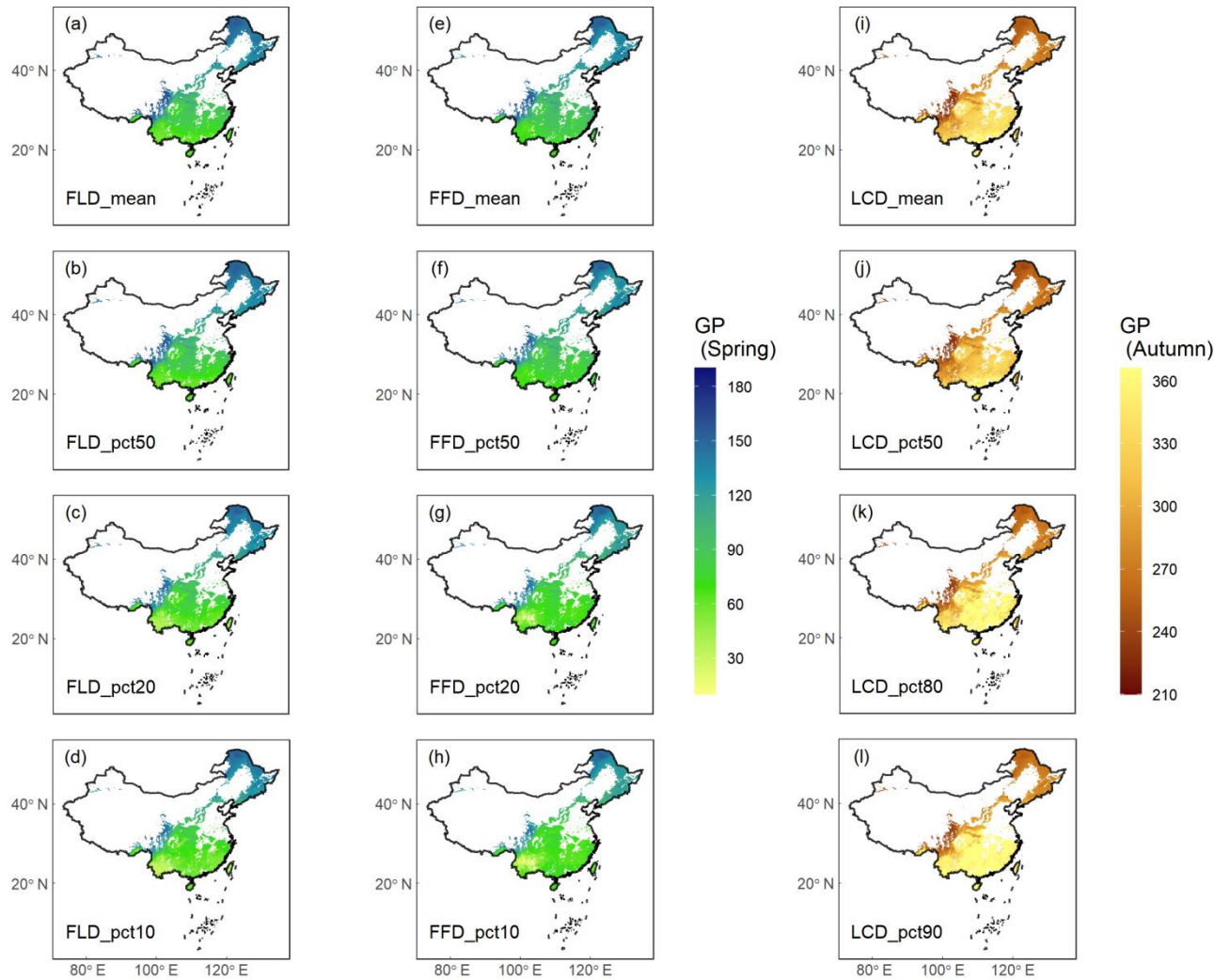


Figure 6: Ground phenology (GP) maps of four aggregation methods averaged from 1951 to 2020. Columns 1-2 show the spring phenophases (FLD and FFD), and Column 3 shows the autumn phenophase (LCD). Each row represents an aggregation method from weighted average (mean), weighted median (pct50), weighted 20% or 80% percentile (pct20\80), and weighted 10% or 90% percentile (pct10\90). The unit of GP is the Julian Day of year (DOY) from January 1st.

We have introduced two types of QA maps to assess the reliability of the aggregated GP maps (Fig. S1). The first QA map represents the total distribution probability of all species considered in the aggregation process, while the second QA map indicates the total number of species that have a distribution probability exceeding 0.1. In these QA maps, higher values correlate with a greater total number or higher cumulative probability of species within the aggregation, which signifies, a higher reliability of GP maps for those particular areas. Notably, the most dependable GP aggregation results are distributed

- 删除[伊洛。]: also
- 删除[伊洛。]: evaluate
- 删除[伊洛。]: ion results of
- 删除[伊洛。]: is
- 删除[伊洛。]: and
- 删除[伊洛。]: is
- 删除[伊洛。]: with
- 删除[伊洛。]: ics
- 删除[伊洛。]: greater than
- 删除[伊洛。]: for
- 删除[伊洛。]: indicating that GP maps
- 删除[伊洛。]: have
- 删除[伊洛。]: in these
- 删除[伊洛。]: The regions with
- 删除[伊洛。]: reliable
- 删除[伊洛。]: were

305 around the 30° N latitude within China. In this region, the total number of species contributing to FLD and FFD is about 15,
306 whereas for LCD, the number is around 6. However, it should be noted that the QA maps also identify areas where the GP
307 aggregation may be less dependable. Specifically, in regions where the total number of species is fewer than 5 or the total
308 probability is below 1, the reliability of the aggregated GP results may be compromised.

309 3.3 Data quality and usability

310 Our comparative analysis between GP and LSP focused on the FLD and SOS in spring, as well as the LCD and EOS in
311 autumn across two periods (1981-2014 and 2013-2020). The results revealed that GP and two LSP products exhibited
312 congruent spatial patterns in central and northern China, while discrepancies were more pronounced in southern China (Fig.
313 7), particularly regarding LCD and EOS in autumn (Fig. 7e-h). This is likely due to the prevalence of deciduous forests in
314 central and northern China (Fig. 1). In contrast, southern China is characterized by a higher presence of evergreen and mixed
315 forests. The GP maps in this study were derived from the phenological data of 24 deciduous woody plants species, which
316 are well-represented in deciduous forests but less so in evergreen or mixed forests. Moreover, LSP metrics obtained from
317 remote sensing data are generally more error-prone in evergreen and mixed forests due to the lack of obvious seasonal
318 change and frequent cloud cover in these regions (Liu et al., 2016b). Consequently, the correlation between GP and LSP in
319 evergreen or mixed forests was found to be relatively weak (Fig. S2), with the highest r being 0.44 in spring and 0.54 in
320 autumn, and the lowest RMSE being 28.5 days in spring and 38.5 days in autumn (Table S2). In deciduous forests, however,
321 the alignment between GP and LSP was substantially stronger, with the highest r being 0.95 in spring and 0.88 in autumn,
322 and the lowest RMSE being 8.8 days in spring and 15.1 days in autumn, respectively.

删除[伊洛。]: T

删除[伊洛。]: for FLD and FFD

删除[伊洛。]: and

删除[伊洛。]: about

删除[伊洛。]: for LCD in these regions

删除[伊洛。]: It should be noted that in the QA map,

删除[伊洛。]: areas

删除[伊洛。]: less

删除[伊洛。]: of species

删除[伊洛。]: less than

删除[伊洛。]: aggregation results of GP may not be reliable

删除[伊洛。]: were compared between

删除[伊洛。]: and between

删除[伊洛。]: during

删除[伊洛。]: segments

删除[伊洛。]: showed

删除[伊洛。]: had similar

删除[伊洛。]: but relatively different patterns

删除[伊洛。]: for

删除[伊洛。]: evergreen and mixed forests are found in

删除[伊洛。]: .

删除[伊洛。]: as

删除[伊洛。]: generated by aggregating

删除[伊洛。]: phenology

删除[伊洛。]: made up a large proportion of

删除[伊洛。]: a small proportion of

删除[伊洛。]: in evergreen or mixed forests

删除[伊洛。]: 1.

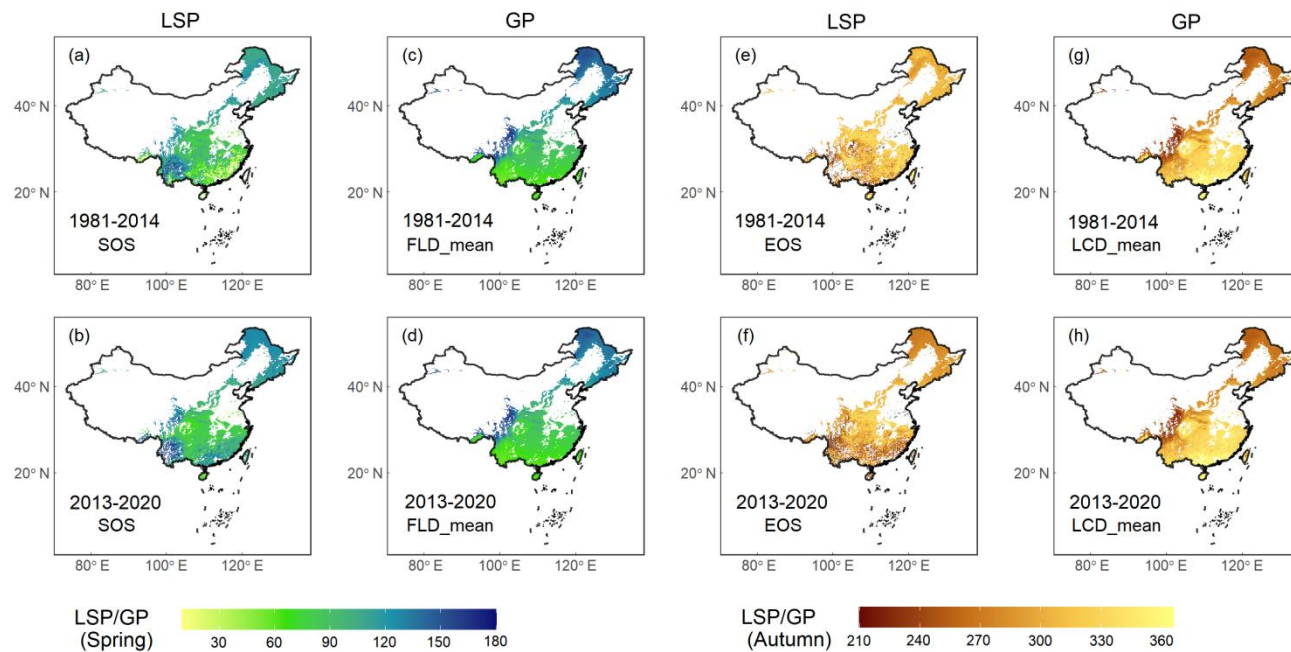


Figure 7: Comparison of GP maps in this study and two LSP products (VIPPHEN and VNP22C2) extracted from remote sensing in previous studies, which was made between FLD and SOS in spring and LCD and EOS in autumn. Row 1 shows the comparison between VIPPHEN product and GP map averaged in 1981-2014, and Row 2 shows the comparison between VNP22C2 product and GP map averaged in 2013-2020. (a-b) SOS from two LSP products; (c-d) FLD aggregated by mean method; (e-f) EOS from two LSP products; (g-h) LCD aggregated by mean method. The unit of GP or LSP is the Julian Day of year (DOY) from January 1st.

To further assess the data quality, we scrutinized the congruence between GP and LSP specifically within deciduous forests. The analysis indicated that GP and LSP exhibit a robust consistency for both VIPPHEN and VNP22C2 products, characterized by strong correlations, minor differences, and solid linear relationships (Fig. 8). The LSP derived from the VIPPHEN product, demonstrated superior consistency with our study's GP compared to the VNP22C2 product's LSP. Furthermore, for both LSP products, the consistency between GP and LSP was significantly better in spring (Fig. 8e, g) than in autumn (Fig. 8f, h). When evaluating the influence of different aggregation methods on the GP and LSP correlation, no significant difference was observed in r among the methods (Fig. 8a, b). The consistency, as measured by r , was comparable across all methods, with values ranging from 0.76-0.78 in spring and 0.49-0.53 in autumn for the VIPPHEN product. For the VNP22C2 product, r values ranging from 0.90-0.91 in spring and 0.79-0.84 in autumn. Contrastingly, the RMSE between GP and LSP varied notably across the different methods (Fig. 8c, d), which is largely attributable to the disparities in the average GP values generated by each method. The most effective aggregation methods, which yielded the smallest RMSE,

删除[伊洛。]: of the data

删除[伊洛。]: examined

删除[伊洛。]: consistency

删除[伊洛。]: Compared with

删除[伊洛。]: t

删除[伊洛。]: of

删除[伊洛。]: ,

删除[伊洛。]: LSP of

删除[伊洛。]: has better consistency with the GP of this ...

删除[伊洛。]: was significantly better

删除[伊洛。]: that

删除[伊洛。]: (mean, pct50, pct20/80, pct10/90)

删除[伊洛。]: there was

删除[伊洛。]: between GP and LSP

设置格式[伊洛。]: 字体: 倾斜

删除[伊洛。]: A

删除[伊洛。]: produced similar r values

删除[伊洛。]: ,

删除[伊洛。]: and

删除[伊洛。]: for the VNP22C2 product

删除[伊洛。]: However

删除[伊洛。]: different methods produced significantly ...

删除[伊洛。]: t

删除[伊洛。]: values

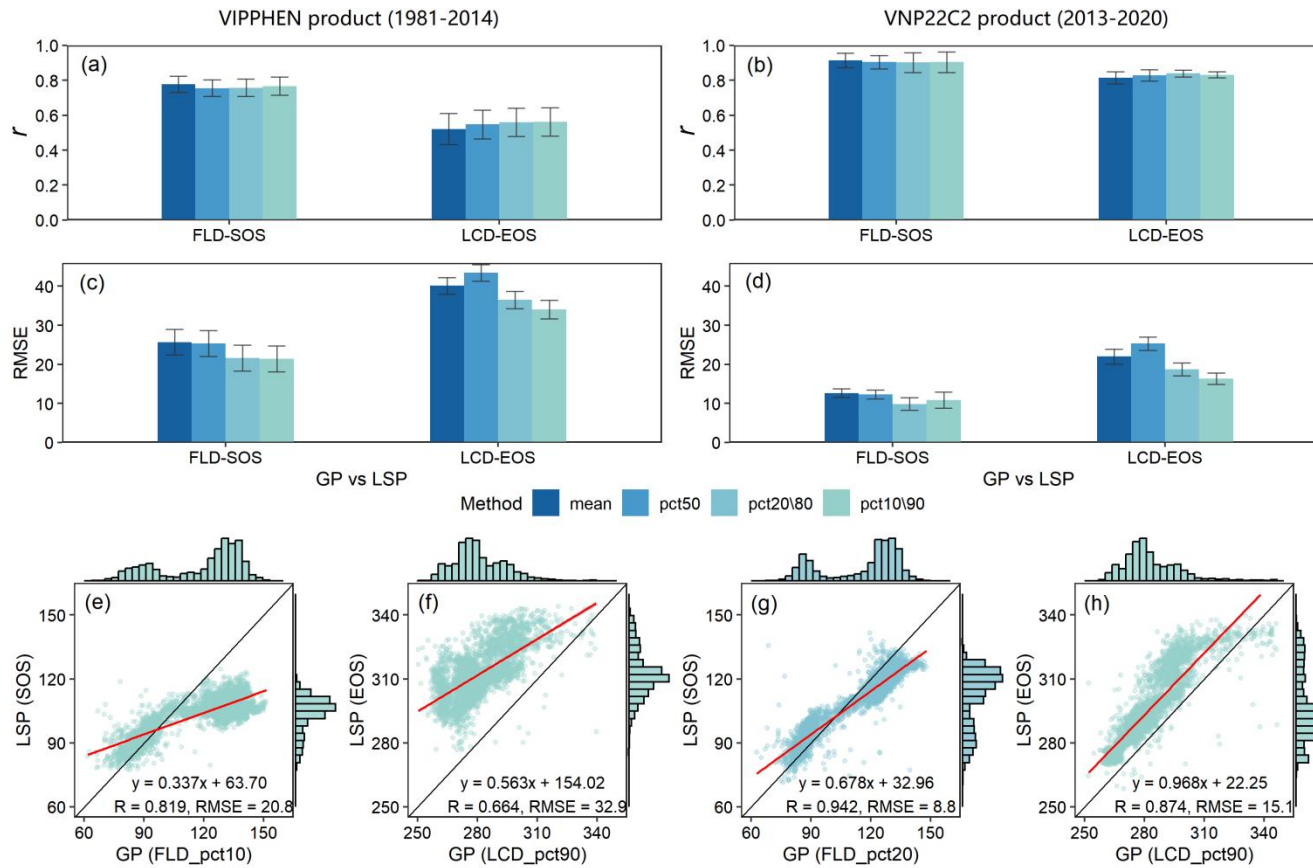
删除[伊洛。]: due

删除[伊洛。]: differences

删除[伊洛。]: of GP under different

删除[伊洛。]: 1. s

342 were pct10 (20.8 days) in spring and pct90 (32.9 days) in autumn for the VIPPHEN product. For the VNP22C2 product,
 343 pct20 (8.8 days) in spring and pct90 (15.1 days) in autumn were identified as the best methods.



344 **Figure 8:** Comparison results of GP maps and two LSP products (VIPPHEN and VNP22C2) in deciduous forests, which
 345 was made between FLD and SOS in spring and LCD and EOS in autumn within the time range 1981-2014 and 2013-2020.
 346 (a-b) r between LSP and GP under four aggregating methods; (c-d) RMSE between LSP and GP under four aggregating
 347 methods; (e-h) Linear relationship between between LSP and GP under the best aggregating method. Each aggregating
 348 method is represented by a different color. The best aggregating method was determined by minimizing the RMSE between
 349 GP and LSP. The error bar in the bar plot represents the multi-year standard deviation. The red line in the scatter plot
 350 represents the linear regression line between GP and LSP, and all regression results were extremely significant ($p < 0.001$).
 351

352 The findings of this study highlight that the most accurate reflection of GP in comparison to LSP from remote sensing
 353 data occurs with the use of the 10th or 20th percentile for spring phenology and the 90th percentile for autumn phenology.
 354 This suggests that the onset of spring as detected by remote sensing aligns more closely with the FLD of the earliest
 355 emerging plant species (the first 10%-20%) on the ground. Conversely, the signal of vegetative dormancy in autumn from

删除[伊洛。]: ,

删除[伊洛。]: and

删除[伊洛。]: for the VNP22C2 product

删除[伊洛。]: It is worth noting

删除[伊洛。]: aggregation method with the smallest
difference between

删除[伊洛。]: and

删除[伊洛。]: in this study was

删除[伊洛。]: in

删除[伊洛。]: in

删除[伊洛。]: It means

删除[伊洛。]: green-up event

删除[伊洛。]: is

删除[伊洛。]: consistent

删除[伊洛。]: earlier-developing

删除[伊洛。]: ,

删除[伊洛。]: while the

删除[伊洛。]: dormancy event

remote sensing is **in greater concordance** with the LCD of **the last** senescent plant species (the last 10%). **These insights are significant because they** reveal a **discernible link** between GP and LSP, despite **inherent differences in how these two types of phenology are measured**. **The consistency between early spring and late autumn events in GP and LSP underscores the potential for integrating these two phenological data sources to enhance our understanding of ecosystem dynamics and the effects of climate change on vegetative cycles.**

The dataset represents a robust compilation of species and ground phenology simulations **for** forests **of** China **over** the past 70 years, **distinguishing itself as** an independent phenological data source **derived from ground observations through** modeling and aggregation. **When applying this data, several factors must be considered:**

(1) For SP maps, the accuracy **is contingent upon the** RMSE and R^2 **resulting from** cross-validation **against** the optimal phenology model for each species (Table 2). Additionally, the **spatial** reliability of phenology data **is influenced** by the **density of observational** sites **per** species (Table 1). For instance, **while the FLD** of *Betula platyphylla*'s **exhibits** high overall **accuracy** (RMSE = 3.80 and $R^2 = 0.915$), the accuracy **may be compromised locally in areas with fewer observation sites** (n = 13). **Across the 24 species studied**, SP maps **consistently aligned** with the in-situ observations, with an average error of 6.4 **days for FLD**, 7.5 **days for FFD**, and 10.8 days **for** LCD. These errors **are comparable or lower** than those **reported in phenological studies from other regions**. For example, simulation error of spring FLD and FFD was 7-9 days in central Europe (Basler, 2016) and was 12.3-12.7 days in the United States (Izquierdo-Verdiguier et al., 2018), while the simulation error of autumn LCD was 10.3-13.0 days in France (Delpierre et al., 2009) and 5.9-22.8 days in the United States (Jeong and Medvigy, 2014). **Consequently**, compared with other studies on the regional scale, the SP maps of China in this study were found to have relatively high accuracy.

(2) For GP maps, **data** reliability can be **assessed using** QA maps, which **reflect** the total number or probability of species. Additionally, reliability can be evaluated by comparing GP **maps** with other LSP products, with **a high degree of** consistency indicating **strong** reliability. **However, it is crucial to note that** GP data **primarily represent** phenological estimates **for** deciduous **forest** components, **resulting in higher** reliability **within** deciduous forests **and lower** within evergreen or mixed forests. In this study, GP maps **for** forests in China **demonstrated strong** consistency with existing LSP products, **especially within** deciduous forests. **The** correlation coefficients of FLD and LCD were 0.91 and 0.84, respectively. **Furthermore, the discrepancies** between GP and LSP **for** FLD and LCD were **relatively minor** in deciduous forests, **at** 8.8 days and 15.1 days, respectively. Previous studies have **reported lower** consistency between **LSP and single** species **phenology**, with correlations ranging from 0.50 to 0.51 in the United States (Peng et al., 2017) and Germany (Kowalski et al., 2020), and **discrepancies spanning** 12 to 14.5 days in the United States (Peng et al., 2017) and Canada (Delbart et al., 2015). **On the other hand**, research comparing **GP aggregates** (average or quantile values) of multiple species has **yielded** better **correlation coefficients**, **ranging from** 0.61 to 0.71 in Europe (Rodriguez-Galiano et al., 2015; Tian et al., 2021), **and** 0.54 to 0.57 **for the 30th percentile GP** in China (Wu et al., 2016). **These studies reported discrepancies** between GP and LSP **of** 10.3-12.4 days in China (Wu et al., 2016), 13.9 days in Europe, and **around** 12.3 days in the United States (Ye et al., 2022), which **are greater** than the FLD **discrepancies** but **less** than **those for** LCD **found in our** study. **While** the

删除[伊洛。]: more consisten

删除[伊洛。]: later-

删除[伊洛。]: on the ground

删除[伊洛。]: results

删除[伊洛。]: potential connection

删除[伊洛。]: s

删除[伊洛。]: s

删除[伊洛。]: their different physical implications in

删除[伊洛。]: In general, this

删除[伊洛。]: provides high reliability

删除[伊洛。]: of

删除[伊洛。]: over

删除[伊洛。]: for

删除[伊洛。]: .

删除[伊洛。]: It is

删除[伊洛。]: y

删除[伊洛。]: generated by

删除[伊洛。]: the

删除[伊洛。]: based on ground observations

删除[伊洛。]: There are several considerations in data

删除[伊洛。]: of data was

删除[伊洛。]: determined by

删除[伊洛。]: of

删除[伊洛。]: on

删除[伊洛。]: in space was

删除[伊洛。]: affected

删除[伊洛。]: number of

删除[伊洛。]: 1: available for modeling on each

391 aggregated GP data derived from species-level phenology data in this study are generally reliable, it's important to recognize
392 that limitations still exist in the available species-specific data, particularly when applied to evergreen or mixed forest
393 regions.

394 (3) For phenology maps in different seasons, the phenology data exhibit significantly higher reliability for spring events
395 compared to those in autumn. The underlying reason is that the biological processes underlying autumn phenology is more
396 complex than those of spring (Menzel, 2002). Moreover, the mechanistic drivers of autumn phenology are intricate, which
397 poses an additional challenge (Gill et al., 2015; Wu et al., 2018). For example, temperature has large effects on the autumn
398 phenology than the spring phenology (Fu et al., 2018). In addition to temperature, other environmental factors such as
399 precipitation (An et al., 2020), photoperiod (Lang et al., 2019), solar radiation (Wu et al., 2021b), spring phenology (Liu et
400 al., 2016a), and growing-season productivity (Zani et al., 2020), also play significant roles in shaping autumn phenology.
401 Given the multiplicity and complexity of these driving mechanisms, modeling autumn phenology becomes a more daunting
402 task (Melaas et al., 2016). As a result, SP and GP maps for autumn manifest lower model performance and data quality
403 relative to their spring counterparts.

404 4 Data availability

405 The annual SP and GP maps over China can be accessed at <https://doi.org/10.57760/sciencedb.07995> (Zhu et al., 2023).
406 This dataset is licensed under a CC-BY 4.0 license. The spatial reference system of the dataset is EPSG:4326(WGS84).

407 5 Conclusions

408 Leveraging historical observations from the CPON, this study introduces a novel, long-term gridded phenology dataset
409 that includes SP maps for 24 woody plants species and GP maps of forests over China, covering the period from 1951 to
410 2020. The dataset features a spatial resolution of 0.1° and a temporal resolution of 1 day. The SP maps were produced using
411 a model-based upscaling method to extend the phenology data from in-situ observations to a regional scale across China.
412 The GP maps were generated by employing weighted average and quantile methods to aggregate phenology data from the
413 species to community and landscape levels. Quality assessments of the dataset indicate an average error for SP maps of 6.9
414 days in spring and 10.8 days in autumn. The smallest discrepancies between the GP maps and existing LSP products is 8.8
415 days for spring and 15.1 days for autumn. Compared to the previous studies (Basler, 2016; Delpierre et al., 2009; Izquierdo-
416 Verdiguier et al., 2018; Jeong and Medvigy, 2014; Tian et al., 2021; Wu et al., 2016; Ye et al., 2022), the SP maps from this
417 research exhibit comparable or smaller simulation errors, and the GP maps show strong concordance with other LSP
418 products, underscoring the dataset's high accuracy and reliability. As the inaugural phenological map set for China, this
419 dataset provides an invaluable tool for discerning the spatial patterns of plant phenology along the geographic gradient (e.g.,
420 longitude, latitude, and altitude). It also enables the examination of temporal trends (e.g., interannual, decadal, and secular)

删除[伊洛。]: landscape-level

删除[伊洛。]: aggregated

删除[伊洛。]: showed good reliability

删除[伊洛。]: available species and different aggregation

删除[伊洛。]: reliability of

删除[伊洛。]: in

删除[伊洛。]: was found to be significantly higher than that

删除[伊洛。]: mechanism of

删除[伊洛。]: compared to

删除[伊洛。]: that

删除[伊洛。]: phenology

删除[伊洛。]: driving mechanisms

删除[伊洛。]: for the

删除[伊洛。]: complex

删除[伊洛。]: may

删除[伊洛。]: drive

删除[伊洛。]: Thus, modeling autumn phenology is more

删除[伊洛。]: ,

删除[伊洛。]:

删除[伊洛。]: ing

删除[伊洛。]: in poorer model performance and inferior

删除[伊洛。]: In this study, mainly based on

删除[伊洛。]: historical phenology observations

删除[伊洛。]: we developed a new

删除[伊洛。]: :

删除[伊洛。]: of

删除[伊洛。]: -

删除[伊洛。]: 1-

421 ~~in~~ plant phenology ~~throughout~~ China. ~~Moreover, the dataset offers critical~~ support for ~~research on the impacts of~~ global
422 change, ~~aids in~~ terrestrial ecosystem ~~modeling~~, and ~~contributes to~~ natural resource management ~~strategies~~.

删除[伊洛。]: of

删除[伊洛。]: across

删除[伊洛。]: T

删除[伊洛。]: can also provide important data

删除[伊洛。]: impact assessment

删除[伊洛。]: simulation

设置格式[伊洛。]: 字体颜色: 自动设置, 非突出显示

423 **Author contribution**

424 QG and JD designed the study and planned the modeling. HW developed the model code. WL and YH performed the
425 simulations. MZ processed the modeling data, performed the computations and drafted the manuscript. JD and JA critically
426 revised the manuscript. All authors discussed and contributed to the modeling and manuscript.

427 **Competing interests**

428 The authors declare that they have no conflict of interest.

429 **Acknowledgements**

430 This study was jointly supported by National Key Research and Development Program of China (2018YFA0606102),
431 National Natural Science Foundation of China (42271062), and Strategic Priority Research Program (A) of Chinese
432 Academy of Sciences (XDA19020303; XDA26010202). Phenology data was provided by CPON. Temperature data was
433 provided by Copernicus Climate Change Service (C3S).

434 **References**

- 435 An, S., Chen, X., Zhang, X., Lang, W., Ren, S., and Xu, L.: Precipitation and minimum temperature are primary climatic
436 controls of alpine grassland autumn phenology on the Qinghai-Tibet Plateau, *Remote Sens.*, 12, 431,
437 <https://doi.org/10.3390/rs12030431>, 2020.
- 438 Aono, Y. and Kazui, K.: Phenological data series of cherry tree flowering in Kyoto, Japan, and its application to
439 reconstruction of springtime temperatures since the 9th century, *Int. J. Climatol.*, 28, 905–914,
440 <https://doi.org/10.1002/joc.1594>, 2008.
- 441 Ault, T. R., Schwartz, M. D., Zurita-Milla, R., Weltzin, J. F., and Betancourt, J. L.: Trends and natural variability of spring
442 onset in the coterminous United States as evaluated by a new gridded dataset of spring indices, *J. Clim.*, 28, 8363–8378,
443 <https://doi.org/10.1175/jcli-d-14-00736.1>, 2015.
- 444 Basler, D.: Evaluating phenological models for the prediction of leaf-out dates in six temperate tree species across central
445 Europe, *Agric. For. Meteorol.*, 217, 10–21, <https://doi.org/10.1016/j.agrformet.2015.11.007>, 2016.

446 Bolton, D. K., Gray, J. M., Melaas, E. K., Moon, M., Eklundh, L., and Friedl, M. A.: Continental-scale land surface
447 phenology from harmonized Landsat 8 and Sentinel-2 imagery, *Remote Sens. Environ.*, 240, 111685,
448 <https://doi.org/10.1016/j.rse.2020.111685>, 2020.

449 Brown, J. H.: On the Relationship between Abundance and Distribution of Species, *Am. Nat.*, 124, 255–279,
450 <https://doi.org/10.1086/284267>, 1984.

451 Brun, P., Zimmermann, N., Hari, C., Pellissier, L., and Karger, D.: CHELSA-BIOCLIM+ A novel set of global climate-
452 related predictors at kilometre-resolution, *EnviDat [data set]*, 10, 2022a.

453 Brun, P., Zimmermann, N. E., Hari, C., Pellissier, L., and Karger, D. N.: Global climate-related predictors at kilometer
454 resolution for the past and future, *Earth Syst. Sci. Data*, 14, 5573–5603, <https://doi.org/10.5194/essd-14-5573-2022>,
455 2022b.

456 Cai, H., Lyu, L., Shrestha, N., Tang, Z., Su, X., Xu, X., Dimitrov, D., and Wang, Z.: Geographical patterns in phylogenetic
457 diversity of Chinese woody plants and its application for conservation planning, *Divers. Distrib.*, 27, 179–194,
458 <https://doi.org/10.1111/ddi.13180>, 2021.

459 Chuine, I.: A unified model for budburst of trees, *J. Theor. Biol.*, 207, 337–347, <https://doi.org/10.1006/jtbi.2000.2178>,
460 2000.

461 Chuine, I., Cour, P., and Rousseau, D.: Fitting models predicting dates of flowering of temperate-zone trees using simulated
462 annealing, *Plant Cell Environ.*, 21, 455–466, <https://doi.org/10.1046/j.1365-3040.1998.00299.x>, 1998.

463 Chuine, I., Cambon, G., and Comtois, P.: Scaling phenology from the local to the regional level: advances from species-
464 specific phenological models, *Global Change Biol.*, 6, 943–952, <https://doi.org/10.1046/j.1365-2486.2000.00368.x>,
465 2000.

466 Cleland, E. E., Chuine, I., Menzel, A., Mooney, H. A., and Schwartz, M. D.: Shifting plant phenology in response to global
467 change, *Trends Ecol. Evol.*, 22, 357–365, <https://doi.org/10.1016/j.tree.2007.04.003>, 2007.

468 Dai, J., Wang, H., and Ge, Q.: Multiple phenological responses to climate change among 42 plant species in Xi’an, China,
469 *Int. J. Biometeorol.*, 57, 749–758, <https://doi.org/10.1007/s00484-012-0602-2>, 2013.

470 Dai, J., Wang, H., and Ge, Q.: Characteristics of spring phenological changes in China over the past 50 years, *Adv.*
471 *Meteorol.*, 2014, 1–8, <https://doi.org/10.1155/2014/843568>, 2014.

472 Delbart, N., Beaubien, E., Kergoat, L., and Le Toan, T.: Comparing land surface phenology with leafing and flowering
473 observations from the PlantWatch citizen network, *Remote Sens. Environ.*, 160, 273–280,
474 <https://doi.org/10.1016/j.rse.2015.01.012>, 2015.

475 Delpierre, N., Dufrière, E., Soudani, K., Ulrich, E., Cecchini, S., Boé, J., and François, C.: Modelling interannual and spatial
476 variability of leaf senescence for three deciduous tree species in France, *Agric. For. Meteorol.*, 149, 938–948,
477 <https://doi.org/10.1016/j.agrformet.2008.11.014>, 2009.

478 Didan, K. and Barreto, A.: NASA MEaSUREs Vegetation Index and Phenology (VIP) Phenology NDVI Yearly Global
479 0.05Deg CMG, NASA EOSDIS Land Processes DAAC, accessed on 2022-08-11,
480 https://doi.org/10.5067/MEaSUREs/VIP/VIPPHEN_NDVI.004, 2016.

481 Dixon, D. J., Callow, J. N., Duncan, J. M., Setterfield, S. A., and Pauli, N.: Satellite prediction of forest flowering
482 phenology, *Remote Sens. Environ.*, 255, 112197, <https://doi.org/10.1016/j.rse.2020.112197>, 2021.

483 Donnelly, A., Yu, R., Jones, K., Belitz, M., Li, B., Duffy, K., Zhang, X., Wang, J., Seyednasrollah, B., Gerst, K. L., and
484 others: Exploring discrepancies between in situ phenology and remotely derived phenometrics at NEON sites,
485 *Ecosphere*, 13, e3912, <https://doi.org/10.1002/ecs2.3912>, 2022.

486 Dronova, I. and Taddeo, S.: Remote sensing of phenology: Towards the comprehensive indicators of plant community
487 dynamics from species to regional scales, *J. Ecol.*, 110, 1460–1484, <https://doi.org/10.1111/1365-2745.13897>, 2022.

488 Estrella, N. and Menzel, A.: Responses of leaf colouring in four deciduous tree species to climate and weather in Germany,
489 *Clim. Res.*, 32, 253–267, <https://doi.org/10.3354/cr032253>, 2006.

490 Fang, J., Wang, Z., and Tang, Z.: Atlas of woody plants in China: distribution and climate, Springer Science & Business
491 Media, 2011.

492 Fielding, A. H. and Bell, J. F.: A review of methods for the assessment of prediction errors in conservation presence/absence
493 models, *Environ. Conserv.*, 24, 38–49, <https://doi.org/10.1017/s0376892997000088>, 1997.

494 Fisher, J. I., Mustard, J. F., and Vadeboncoeur, M. A.: Green leaf phenology at Landsat resolution: Scaling from the field to
495 the satellite, *Remote Sens. Environ.*, 100, 265–279, <https://doi.org/10.1016/j.rse.2005.10.022>, 2006.

496 Fitchett, J. M., Grab, S. W., and Thompson, D. I.: Plant phenology and climate change: Progress in methodological
497 approaches and application, *Prog. Phys. Geogr.*, 39, 460–482, <https://doi.org/10.1177/0309133315578940>, 2015.

498 Friedl, M. and Sulla-Menashe, D.: MODIS/Terra+Aqua Land Cover Type Yearly L3 Global 500m SIN Grid V061, NASA
499 EOSDIS Land Processes DAAC, <https://doi.org/10.5067/MODIS/MCD12Q1.061>, 2022.

500 Fu, Y., Li, X., Zhou, X., Geng, X., Guo, Y., and Zhang, Y.: Progress in plant phenology modeling under global climate
501 change, *Sci. China Earth Sci.*, 63, 1237–1247, <https://doi.org/10.1007/s11430-019-9622-2>, 2020.

502 Fu, Y. H., Zhao, H., Piao, S., Peaucelle, M., Peng, S., Zhou, G., Ciais, P., Huang, M., Menzel, A., Peñuelas, J., and others:
503 Declining global warming effects on the phenology of spring leaf unfolding, *Nature*, 526, 104–107,
504 <https://doi.org/10.1038/nature15402>, 2015.

505 Fu, Y. H., Piao, S., Delpierre, N., Hao, F., Hänninen, H., Liu, Y., Sun, W., Janssens, I. A., and Campioli, M.: Larger
506 temperature response of autumn leaf senescence than spring leaf-out phenology, *Global Change Biol.*, 24, 2159–2168,
507 <https://doi.org/10.1111/gcb.14021>, 2018.

508 GBIF: GBIF Occurrence Download, accessed on 2022-08-12, <https://doi.org/10.15468/dl.7dwjev>, 2022.

509 Ge, Q., Wang, H., and Dai, J.: Simulating changes in the leaf unfolding time of 20 plant species in China over the twenty-
510 first century, *Int. J. Biometeorol.*, 58, 473–484, <https://doi.org/10.1007/s00484-013-0671-x>, 2014.

511 Ge, Q., Wang, H., Rutishauser, T., and Dai, J.: Phenological response to climate change in China: a meta-analysis, *Global*
512 *Change Biol.*, 21, 265–274, <https://doi.org/10.1111/gcb.12648>, 2015.

513 Gill, A. L., Gallinat, A. S., Sanders-DeMott, R., Rigden, A. J., Short Gianotti, D. J., Mantooth, J. A., and Templer, P. H.:
514 Changes in autumn senescence in northern hemisphere deciduous trees: a meta-analysis of autumn phenology studies,
515 *Ann Bot*, 116, 875–888, <https://doi.org/10.1093/aob/mcv055>, 2015.

516 Hufkens, K., Basler, D., Milliman, T., Melaas, E. K., and Richardson, A. D.: An integrated phenology modelling framework
517 in R, *Methods Ecol. Evol.*, 9, 1276–1285, <https://doi.org/10.1111/2041-210x.12970>, 2018.

518 Izquierdo-Verdiguier, E., Zurita-Milla, R., Ault, T. R., and Schwartz, M. D.: Development and analysis of spring plant
519 phenology products: 36 years of 1-km grids over the conterminous US, *Agric. For. Meteorol.*, 262, 34–41,
520 <https://doi.org/10.1016/j.agrformet.2018.06.028>, 2018.

521 Jeong, S.-J. and Medvigy, D.: Macroscale prediction of autumn leaf coloration throughout the continental United States,
522 *Global Ecol. Biogeogr.*, 23, 1245–1254, <https://doi.org/10.1111/geb.12206>, 2014.

523 Keenan, T. F., Gray, J., Friedl, M. A., Toomey, M., Bohrer, G., Hollinger, D. Y., Munger, J. W., O’Keefe, J., Schmid, H. P.,
524 Wing, I. S., and others: Net carbon uptake has increased through warming-induced changes in temperate forest
525 phenology, *Nat. Clim. Change*, 4, 598–604, <https://doi.org/10.1038/nclimate2253>, 2014.

526 Kowalski, K., Senf, C., Hostert, P., and Pflugmacher, D.: Characterizing spring phenology of temperate broadleaf forests
527 using Landsat and Sentinel-2 time series, *Int. J. Appl. Earth Obs. Geoinf.*, 92, 102172,
528 <https://doi.org/10.1016/j.jag.2020.102172>, 2020.

529 Lang, W., Chen, X., Qian, S., Liu, G., and Piao, S.: A new process-based model for predicting autumn phenology: how is
530 leaf senescence controlled by photoperiod and temperature coupling?, *Agric. For. Meteorol.*, 268, 124–135,
531 <https://doi.org/10.1016/j.agrformet.2019.01.006>, 2019.

532 Li, X., Zhou, Y., Meng, L., Asrar, G. R., Lu, C., and Wu, Q.: A dataset of 30 m annual vegetation phenology indicators
533 (1985–2015) in urban areas of the conterminous United States, *Earth Syst. Sci. Data*, 11, 881–894,
534 <https://doi.org/10.5194/essd-11-881-2019>, 2019.

535 Liang, L., Schwartz, M. D., and Fei, S.: Validating satellite phenology through intensive ground observation and landscape
536 scaling in a mixed seasonal forest, *Remote Sens. Environ.*, 115, 143–157, <https://doi.org/10.1016/j.rse.2010.08.013>,
537 2011.

538 Lieth, H.: Purposes of a phenology book, in: *Phenology and Seasonality Modeling*, edited by: Lieth, H., Springer, Berlin,
539 Heidelberg, 3–19, https://doi.org/10.1007/978-3-642-51863-8_1, 1974.

540 Liu, H., Gong, P., Wang, J., Clinton, N., Bai, Y., and Liang, S.: Annual dynamics of global land cover and its long-term
541 changes from 1982 to 2015, *Earth Syst. Sci. Data*, 12, 1217–1243, <https://doi.org/10.5194/essd-12-1217-2020>, 2020.

542 Liu, Q., Fu, Y. H., Zhu, Z., Liu, Y., Liu, Z., Huang, M., Janssens, I. A., and Piao, S.: Delayed autumn phenology in the
543 Northern Hemisphere is related to change in both climate and spring phenology, *Global Change Biol.*, 22, 3702–3711,
544 <https://doi.org/10.1111/gcb.13311>, 2016a.

545 Liu, Y., Wu, C., Peng, D., Xu, S., Gonsamo, A., Jassal, R. S., Arain, M. A., Lu, L., Fang, B., and Chen, J. M.: Improved
546 modeling of land surface phenology using MODIS land surface reflectance and temperature at evergreen needleleaf
547 forests of central North America, *Remote Sens. Environ.*, 176, 152–162, <https://doi.org/10.1016/j.rse.2016.01.021>,
548 2016b.

549 Melaas, E. K., Sulla-Menashe, D., Gray, J. M., Black, T. A., Morin, T. H., Richardson, A. D., and Friedl, M. A.: Multisite
550 analysis of land surface phenology in North American temperate and boreal deciduous forests from Landsat, *Remote*
551 *Sens. Environ.*, 186, 452–464, <https://doi.org/10.1016/j.rse.2016.09.014>, 2016.

552 Menzel, A.: Phenology: its importance to the global change community, *Clim. Change*, 54, 379,
553 <https://doi.org/10.1023/A:1016125215496>, 2002.

554 Menzel, A., Yuan, Y., Matiu, M., Sparks, T., Scheffinger, H., Gehrig, R., and Estrella, N.: Climate change fingerprints in
555 recent European plant phenology, *Global Change Biol.*, 26, 2599–2612, <https://doi.org/10.1111/gcb.15000>, 2020.

556 Misra, G., Cawkwell, F., and Wingler, A.: Status of phenological research using Sentinel-2 data: A review, *Remote Sens.*,
557 12, 2760, <https://doi.org/10.3390/rs12172760>, 2020.

558 Muñoz Sabater, J.: ERA5-Land hourly data from 1981 to present, Copernicus Climate Change Service (C3S) Climate Data
559 Store (CDS), 2019.

560 Muñoz Sabater, J.: ERA5-Land hourly data from 1950 to 1980, Copernicus Climate Change Service (C3S) Climate Data
561 Store (CDS), 2021.

562 Muñoz-Sabater, J., Dutra, E., Agustí-Panareda, A., Albergel, C., Arduini, G., Balsamo, G., Boussetta, S., Choulga, M.,
563 Harrigan, S., Hersbach, H., and others: ERA5-Land: A state-of-the-art global reanalysis dataset for land applications,
564 *Earth Syst. Sci. Data*, 13, 4349–4383, <https://doi.org/10.5194/essd-13-4349-2021>, 2021.

565 Park, D. S., Newman, E. A., and Breckheimer, I. K.: Scale gaps in landscape phenology: challenges and opportunities,
566 *Trends Ecol. Evol.*, 36, 709–721, <https://doi.org/10.1016/j.tree.2021.04.008>, 2021.

567 Peng, D., Wu, C., Li, C., Zhang, X., Liu, Z., Ye, H., Luo, S., Liu, X., Hu, Y., and Fang, B.: Spring green-up phenology
568 products derived from MODIS NDVI and EVI: Intercomparison, interpretation and validation using National Phenology
569 Network and AmeriFlux observations, *Ecol. Indic.*, 77, 323–336, <https://doi.org/10.1016/j.ecolind.2017.02.024>, 2017.

570 Phillips, S. J., Anderson, R. P., and Schapire, R. E.: Maximum entropy modeling of species geographic distributions, *Ecol.*
571 *Modell.*, 190, 231–259, <https://doi.org/10.1016/j.ecolmodel.2005.03.026>, 2006.

572 Piao, S., Liu, Q., Chen, A., Janssens, I. A., Fu, Y., Dai, J., Liu, L., Lian, X., Shen, M., and Zhu, X.: Plant phenology and
573 global climate change: Current progresses and challenges, *Glob Chang Biol*, 25, 1922–1940,
574 <https://doi.org/10.1111/gcb.14619>, 2019.

575 Polgar, C. A. and Primack, R. B.: Leaf-out phenology of temperate woody plants: from trees to ecosystems, *New Phytol.*,
576 191, 926–941, <https://doi.org/10.1111/j.1469-8137.2011.03803.x>, 2011.

577 Pukelsheim, F.: The three sigma rule, *Am. Stat.*, 48, 88–91, <https://doi.org/10.2307/2684253>, 1994.

578 Richardson, A. D., Keenan, T. F., Migliavacca, M., Ryu, Y., Sonnentag, O., and Toomey, M.: Climate change, phenology,
579 and phenological control of vegetation feedbacks to the climate system, *Agric. For. Meteorol.*, 169, 156–173,
580 <https://doi.org/10.1016/j.agrformet.2012.09.012>, 2013.

581 Richardson, A. D., Hufkens, K., Milliman, T., Aubrecht, D. M., Chen, M., Gray, J. M., Johnston, M. R., Keenan, T. F.,
582 Klosterman, S. T., Kosmala, M., and others: Tracking vegetation phenology across diverse North American biomes
583 using PhenoCam imagery, *Sci. Data*, 5, 1–24, <https://doi.org/10.1038/sdata.2018.28>, 2018.

584 Rodriguez-Galiano, V., Dash, J., and Atkinson, P. M.: Intercomparison of satellite sensor land surface phenology and ground
585 phenology in Europe, *Geophys. Res. Lett.*, 42, 2253–2260, <https://doi.org/10.1002/2015gl063586>, 2015.

586 Sagarin, R. D. and Gaines, S. D.: The ‘abundant centre’ distribution: to what extent is it a biogeographical rule?, *Ecol. Lett.*,
587 5, 137–147, <https://doi.org/10.1046/j.1461-0248.2002.00297.x>, 2002.

588 Schwartz, M. D.: *Phenology: an integrative environmental science*, Springer, 2003.

589 Studer, S., Stöckli, R., Appenzeller, C., and Vidale, P. L.: A comparative study of satellite and ground-based phenology, *Int.*
590 *J. Biometeorol.*, 51, 405–414, <https://doi.org/10.1007/s00484-006-0080-5>, 2007.

591 Tang, J., Körner, C., Muraoka, H., Piao, S., Shen, M., Thackeray, S. J., and Yang, X.: Emerging opportunities and
592 challenges in phenology: a review, *Ecosphere*, 7, e01436, <https://doi.org/10.1002/ecs2.1436>, 2016.

593 Tao, Z., Wang, H., Dai, J., Alatalo, J., and Ge, Q.: Modeling spatiotemporal variations in leaf coloring date of three tree
594 species across China, *Agric. For. Meteorol.*, 249, 310–318, <https://doi.org/10.1016/j.agrformet.2017.10.034>, 2018.

595 Templ, B., Koch, E., Bolmgren, K., Ungersböck, M., Paul, A., Scheifinger, H., Rutishauser, T., Busto, M., Chmielewski, F.-
596 M., Hájková, L., and others: Pan European Phenological database (PEP725): a single point of access for European data,
597 *Int. J. Biometeorol.*, 62, 1109–1113, <https://doi.org/10.1007/s00484-018-1512-8>, 2018.

598 Tian, F., Cai, Z., Jin, H., Hufkens, K., Scheifinger, H., Tagesson, T., Smets, B., Van Hoolst, R., Bonte, K., Ivits, E., and
599 others: Calibrating vegetation phenology from Sentinel-2 using eddy covariance, PhenoCam, and PEP725 networks
600 across Europe, *Remote Sens. Environ.*, 260, 112456, <https://doi.org/10.1016/j.rse.2021.112456>, 2021.

601 Wang, H., Dai, J., and Ge, Q.: The spatiotemporal characteristics of spring phenophase changes of *Fraxinus chinensis* in
602 China from 1952 to 2007, *Sci. China Earth Sci.*, 55, 991–1000, <https://doi.org/10.1007/s11430-011-4349-0>, 2012.

603 Wang, H., Wu, C., Ciais, P., Peñuelas, J., Dai, J., Fu, Y., and Ge, Q.: Overestimation of the effect of climatic warming on
604 spring phenology due to misrepresentation of chilling, *Nat. Commun.*, 11, 4945, [https://doi.org/10.1038/s41467-020-](https://doi.org/10.1038/s41467-020-18743-8)
605 18743-8, 2020.

606 Wu, C., Hou, X., Peng, D., Gonsamo, A., and Xu, S.: Land surface phenology of China’s temperate ecosystems over 1999–
607 2013: Spatial–temporal patterns, interaction effects, covariation with climate and implications for productivity,
608 *Agricultural and Forest Meteorology*, 216, 177–187, <https://doi.org/10.1016/j.agrformet.2015.10.015>, 2016.

609 Wu, C., Wang, X., Wang, H., Ciais, P., Peñuelas, J., Myneni, R. B., Desai, A. R., Gough, C. M., Gonsamo, A., Black, A. T.,
610 and others: Contrasting responses of autumn-leaf senescence to daytime and night-time warming, *Nat. Clim. Change*, 8,
611 1092–1096, <https://doi.org/10.1038/s41558-018-0346-z>, 2018.

612 Wu, W., Sun, Y., Xiao, K., and Xin, Q.: Development of a global annual land surface phenology dataset for 1982–2018 from
613 the AVHRR data by implementing multiple phenology retrieving methods, *Int. J. Appl. Earth Obs. Geoinf.*, 103,
614 102487, <https://doi.org/10.1016/j.jag.2021.102487>, 2021a.

615 Wu, Z., Chen, S., De Boeck, H. J., Stenseth, N. C., Tang, J., Vitasse, Y., Wang, S., Zohner, C., and Fu, Y. H.: Atmospheric
616 brightening counteracts warming-induced delays in autumn phenology of temperate trees in Europe, *Global Ecol.*
617 *Biogeogr.*, 30, 2477–2487, <https://doi.org/10.1111/geb.13404>, 2021b.

618 Ye, Y., Zhang, X., Shen, Y., Wang, J., Crimmins, T., and Scheifinger, H.: An optimal method for validating satellite-derived
619 land surface phenology using in-situ observations from national phenology networks, *ISPRS J. Photogramm. Remote*
620 *Sens.*, 194, 74–90, <https://doi.org/10.1016/j.isprsjprs.2022.09.018>, 2022.

621 Zani, D., Crowther, T. W., Mo, L., Renner, S. S., and Zohner, C. M.: Increased growing-season productivity drives earlier
622 autumn leaf senescence in temperate trees, *Science*, 370, 1066–1071, <https://doi.org/10.1126/science.abd8911>, 2020.

623 Zhang, X., Wang, J., Gao, F., Liu, Y., Schaaf, C., Friedl, M., Yu, Y., Jayavelu, S., Gray, J., Liu, L., and others: Exploration
624 of scaling effects on coarse resolution land surface phenology, *Remote Sens. Environ.*, 190, 318–330,
625 <https://doi.org/10.1016/j.rse.2017.01.001>, 2017.

626 Zhang, X., Friedl, M., and Henebry, G.: VIIRS/NPP Land Cover Dynamics Yearly L3 Global 0.05 Deg CMG V001, NASA
627 EOSDIS Land Processes DAAC, accessed on 2022-08-11, <https://doi.org/10.5067/VIIRS/VNP22C2.001>, 2020.

628 Zhu, M., Dai J.: Species phenology and ground phenology maps over China from 1951-2020, Science Data Bank [data set],
629 <https://doi.org/10.57760/sciencedb.07995>. DOI:10.57760/sciencedb.07995, 2023.